ELECTRON AND POSITRON STORAGE RINGS

A. I. ALIKHANYAN, S. A. KHEĬFETS, and S. K. ESIN

Usp. Fiz. Nauk 81, 7-49 (September, 1963)

INTRODUCTION

IT is known that modern quantum electrodynamics is not sufficiently rigorous or free of contradictions. Although the results of calculations based on this theory are confirmed by the experimental data within the limits of errors, the calculation methods do not follow from the theory and are merely special prescriptions. It is frequently necessary to perform during the course of the calculations incorrect operations such as the subtraction of infinitely large quantities. The theory is incapable of calculating some important constants, for example the electron mass, which must be obtained by experiment, etc.[1,2].

The widespread opinion is that these difficulties of the theory result from insufficient knowledge of the structure of space at very short distances, or of the character of the interaction between particles at very high energies.

One of the most highly promising methods of investigating these problems is to study the processes occurring upon collision of high-energy electrons with electrons or positrons of similarly high energy. For a practical realization of experiments of this type it is necessary to have an installation in which one can store large currents of electrons and positrons moving in opposition to each other and to effect collisions between them[3-7].

Such a device, called for brevity a storage ring, can be effected in various ways. In the present review we confine ourselves to storage rings proper, in which no particles are accelerated. We thus set aside problems of storage in devices such as the ring-type proton synchrotron[8-11]. In addition, we shall not deal with the storage of protons, since these questions have nowhere gone beyond the stage of preliminary development[12] and modeling[13,14,60] (see Sec. 4 of Chapter IV).

However, the significance of storage rings for electrons and positrons is not confined to the foregoing possibility of searching for the limits of applicability of quantum electrodynamics. They can serve as inestimable sources of information on the form factors of elementary particles for momentum transfers which will not soon be attainable with accelerators. Storage rings might turn out to be beyond competition with other methods in the investigation of interactions between secondary particles produced upon collisions of electrons and positrons. In particular, because of the negligible relative energy scatter, the resolution of various close-lying resonances in elementary-particle systems can be made particularly accurate.

Finally, storage rings can be used also to perform experiments involving the scattering of electrons and positrons by stationary targets, in which very large currents, not attainable with accelerators, are required.

The bright prospects offered by the use of storage rings have excited tremendous interest. In a large number of laboratories storage rings for electrons and positrons, designed for various energies of the stored particles, are under design or construction. We consider below the principal problems connected with the storage of electrons and positrons.

I. PHYSICAL PRINCIPLES OF EXPERIMENTS IN COLLIDING BEAMS

1. Momentum Transferred in Collisions

Investigations of interactions between elementary particles have been carried out hitherto in such a way that one of the particles was practically at rest in the laboratory frame prior to collision. In this case part of the energy of the colliding particles, connected with the motion of their center of mass, is not used in the reaction. The c.m.s. energy of the particle (for $E_l \gg mc^2$) is equal to

$$E = \sqrt{\frac{mc^2 E_l}{2}}, \qquad (1.1)$$

where E_l is the energy of the incident particle in the laboratory system, mc^2 is the rest energy of the target particle. We see therefore that when an incoming particle of high energy E_l collides with a light particle, only a negligible part of its energy is used. Thus, when an electron with energy $E_l \approx 6$ BeV collides with an electron at rest E is of the order of 40 MeV.

At the present time a real possibility has arisen of

investigating collisions in which both interacting particles move towards each other in the laboratory frame. If their momenta are equal in magnitude, then the laboratory frame coincides with the c.m.s. and the entire particle energy is used in the reaction, $E_l = E$. To obtain in the c.m.s. an energy E equal, say, to 1.5 BeV, an electron colliding with another electron at rest must be accelerated to

$$E_l = \frac{2E^2}{mc^2} . \qquad (1.2)$$

Hence $E_l \approx 9 \times 10^3$ BeV. Such an energy cannot be attained (at least for the time being) with an accelerator. Therefore experiments with colliding electron beams are at present the only way of investigating collisions between light particles where the momentum transfer is on the order of several BeV/c and more.

In experiments with such a momentum transfer, deviations from existing theories may be observed because of violation of quantum electrodynamics at short distances, due to the existence of an elementary length or due to some other types of non-locality of the interaction.

In Table I are listed the minimal distances down to which the structure of the interactions can be investigated at different particle energies and experimental accuracies [15].

Table I. Effective distances (in units of 10^{-13} cm) measurable at given experimental accuracies and colliding-particle energies

$d\sigma/\sigma$ \ E, MeV	100	500	1500	4500
0.10	0.44	0.09	0.030	0.010
0.05	0.32	0.06	0.020	0.007
0.03	0.24	0.05	0.015	0.005
0.01	0.14	0.03	0.010	0.003

2. Principal Processes Occurring in Electron-positron Collisions

Let us consider the processes that occur when electrons collide with electrons or with positrons at high energies. We are now interested only in the cross sections of the processes, and also in their dependence on the energies and on the angles. More detailed information can be found in [16-27]. In the collision between an electron and an electron, principal interest is attached to elastic scattering. Figure 1 and Table II show the values of the differential elastic-scattering cross section for different energies and for different electron scattering angles θ (calculated without radiative corrections and possible form factors).

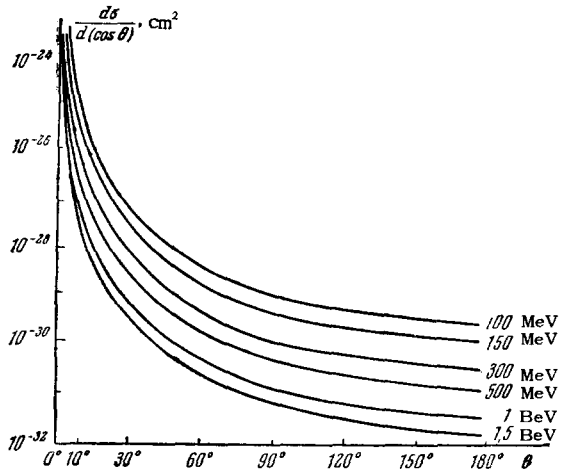

FIG. 1. Differential cross section for elastic electron-electron scattering for different c.m.s. energies of the incoming particles.

In electron-electron collisions, the inelastic processes occur in a higher approximation in $e^2/\hbar c$. Nonetheless, if the transferred 4-momentum is sufficiently small, the cross section for the inelastic process can become sufficiently large. It is necessary, however, to bear in mind that kinematically these processes are much more complicated than the processes, considered below, of the production of the same particles upon annihilation of an electron-positron pair. Furthermore, they must be investigated by working in a narrow solid angle about the direction of motion of the beams.

Electron-positron collisions offer much wider possibilities. The e^+e^- system is neutral in all the "charges" (electric, baryon, lepton, and strangeness). In collisions between electrons and positrons, a great variety of reactions can occur, accompanied by production of particle-antiparticle pairs and of particles which are neutral in all the foregoing "charges" (π^0, γ).

Table II. Differential cross section (cm^2) of elastic Coulomb electron-electron scattering, $d\sigma/d\Omega$, at different energies E of the incoming particles and at different scattering angles θ

E, MeV	θ=10°	θ=30°	θ=60°	θ=90°
500	$3.46 \cdot 10^{-28}$	$4.45 \cdot 10^{-30}$	$3.75 \cdot 10^{-31}$	$1.8 \cdot 10^{-31}$
1000	$8.65 \cdot 10^{-29}$	$1.11 \cdot 10^{-30}$	$9.4 \cdot 10^{-32}$	$4.5 \cdot 10^{-32}$
1500	$3.85 \cdot 10^{-29}$	$4.95 \cdot 10^{-31}$	$4.17 \cdot 10^{-32}$	$2.0 \cdot 10^{-32}$
2000	$2.16 \cdot 10^{-29}$	$2.78 \cdot 10^{-31}$	$2.34 \cdot 10^{-32}$	$1.1 \cdot 10^{-32}$

Table III. Effective cross sections of the reactions occurring upon collision between electrons and positrons (mc^2, μc^2 — rest energies of the electron and secondary particle, κ — anomalous magnetic moment of the baryon)

Reaction	Reaction threshold, MeV	Estimates of differential cross sections $d\sigma/d\Omega$ for the emission of particles at $\theta = 90°$, cm^2/sr
$\gamma+\gamma$	None	$2.0\cdot10^{-26}\ (mc^2/E)^2$
e^-+e^+	None	$4.5\cdot10^{-26}\ (mc^2/E)^2$
$\mu^-+\mu^+$	103	$0.5\cdot10^{-26}\left(\frac{mc^2}{E}\right)^2\left[1-\left(\frac{\mu c^2}{E}\right)^2\right]^{1/2}\times\left[1+\left(\frac{\mu c^2}{E}\right)^2\right]$
$\pi^-+\pi^+$ K^-+K^+ $K^0+\overline{K}^0$	140 470 470	$2.5\cdot10^{-27}\left(\frac{mc^2}{E}\right)^2\left[1-\left(\frac{\mu c^2}{E}\right)^2\right]^{3/2}$
$\pi^0+\gamma$	70	$2.75\cdot10^{-35}\left[1-\left(\frac{\mu c^2}{2E}\right)^2\right]^3$
$N+\overline{N}$	940	$10^{-26}\left(\frac{mc^2}{E}\right)^2\left[1-\left(\frac{\mu c^2}{E}\right)^2\right]^{1/2}(1+\varkappa)^2$

In Table III are listed the main reactions, their thresholds, and estimates for the differential cross sections, calculated without account of the form factors. A characteristic feature of almost all the cross sections is that they decrease with energy as $(mc^2/E)^2$.

A kinematic analysis of these reactions, particularly two-particle reactions, is exceedingly simple. A study of these reactions can yield information on the limits of applicability of quantum electrodynamics [15], on values of the electromagnetic form factors of different elementary particles for timelike momentum transfers, data on the interactions between the secondary particles themselves (particularly resonances and bound states of strongly-interacting particles) [23]. Finally, new unknown particles may be created in collisions between electrons and positrons.

3. Energy of Stored Particles

The choice of energy of the stored particles is affected by many factors. From the point of view of the experimental capabilities with colliding beams, the energy of the storage ring should be as high as possible. There are obvious factors, however, limiting this energy. First, the already noticed tendency of all cross sections to decrease with increasing energy as $(mc^2/E)^2$. The collision probability, which is proportional to the cross section, becomes so small at high energies that the realization of experiments at such energies encounters unsurmountable difficulties. Second, in connection with the presence of synchrotron radiation, the intensity of which increases like $(E/mc^2)^4$ at a given radius of curvature of particle trajectory, the dimensions and cost of the apparatus increase very rapidly. Third, there are no sources of electrons and positrons accelerated to very high energies.

Figure 2, in which production thresholds have been marked on the abscissa axis, shows that to investigate

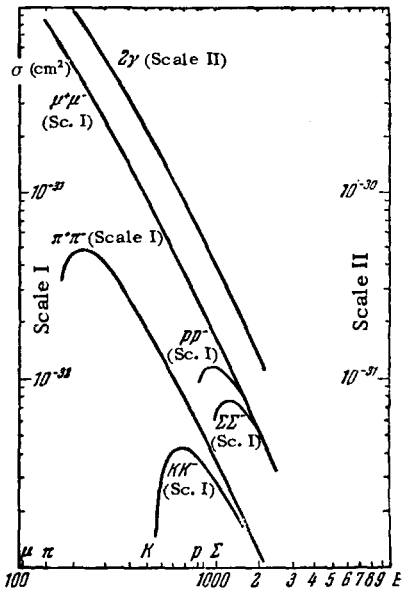

FIG. 2. Total cross sections for the production of elementary particles at different c.m.s. energies of the incoming electrons.

the production of the known elementary particles the storage-ring energy should be ~ 1.5 BeV.

For research with the widest scope, it is necessary to be able to measure the cross sections at different energies of the colliding particles over a wide range of energy variation. The deviation of the experimental cross sections, as functions of the energy, from the calculated values can indicate violation of quantum electrodynamics, and also disclose the physical causes of such violations. Maxima on the experimental cross section vs. energy curve can correspond to various resonances in the interactions of the secondary particles with each other. The width of the maximum yields direct information on the lifetime of the "resonance." In this connection we note that of all the known instruments, the storage ring has the best energy res-

olution. The relative energy scatter in the storage-ring beam can be better than 10^{-3}. This makes it particularly promising for the separation of resonances that lie close to each other.

II. PRINCIPAL STORAGE RING CONSTRUCTIONS

1. Comparison with Accelerators

A device for the storage of electrons is similar in its main outlines to an accelerator of one type or another. Like the accelerator, the storage ring has a magnetic track to shape the beam. An electric field of required frequency is produced in the storage ring to compensate for the energy lost to radiation. The storage ring has injection devices for the capture of the particles in the stable mode, etc.

Depending on the signs of the charges of the colliding beams, the type of the magnetic system, and the method of injection of the particles into the storage ring, different storage schemes are possible. The principal among them are the following.

a) Storage ring for colliding electrons. For the collision of particles of like charge it is necessary to accumulate them in two annular tracks (we disregard systems with two equilibrium orbits, of the annular fm cyclotron type).

An example of a storage ring with two magnetic tracks is the Stanford electron storage ring, the diagram of which is shown in Fig. 9. The electrons can move in each of the tracks either in one direction (with identical direction of the magnetic field), or in opposite directions ("figure eight"). In the second case it is sufficient to have one injection device in place of two.

b) Storage ring for electrons and positrons. Since a positron moving in a magnetic field in a direction opposite to that of an electron is acted upon by the same force, the closed orbits of the electrons and of the positrons moving in opposition to them coincide. Therefore a single magnetic track is sufficient for the storage of electrons and positrons.

c) Finally, schemes wherein the storage occurs directly in the accelerator are possible. One such possibility is to use a symmetrical annular fm cyclotron, in which it is possible to accelerate particles of opposite signs simultaneously and to store them at an outer radius [28-30]. Another possibility is the use of a synchrotron in which the magnetization current exceeds the amplitude of the alternating component of the current [31,32]. We shall not consider these possibilities.

In spite of the great outward similarity to an accelerator, a storage ring has many essential features which greatly distinguish it from an accelerator. The principal feature of storage rings is the very high particle density with very small beam dimensions. This results in the electromagnetic interactions between the particle clusters acquiring very great significance in storage rings. A striking difference between accelerators and storage rings is also to be found in the role of the particle losses in single and multiple processes. Whereas in the accelerator the decisive role is played by multiple processes (quantum fluctuations of radiation, multiple Coulomb scattering), in the storage ring the lifetime of the beam is determined essentially by the single bremsstrahlung and single elastic scattering. The reason for this difference consists in the following: the parameters of the accelerator are chosen such as to ensure smallness of the losses over a relatively short acceleration time. This time is usually much shorter than the lifetime with respect to single processes. Under these conditions, the decisive role in particle loss is played by multiple processes. This is all the more correct since the acceleration cycle begins at relatively low energy; when the scattering cross section is large, there is no radiative damping, and the beam dimensions are comparable with the dimensions of the operating region.

Injection into a storage ring is usually at high particle energy. Radiative damping acts during the entire lifetime of the beam; the beam dimensions soon become much smaller than the permissible stability-region dimensions. Therefore the time of retention of the beam in the storage ring is determined by single processes.

The main units of the storage ring also possess many essential features that distinguish it from accelerators. These differences are due to the natural tendency to build the storage ring in such a way that the interaction probability be maximal during beam collision.

2. Magnetic System

The magnetic system of the storage ring must satisfy many requirements in order for the ring to operate successfully. Although formally these requirements are the same as for accelerators (stability of transverse oscillations, damping of all three types of oscillations), they have their own peculiarities when applied to storage rings. For example, the electromagnetic interaction between the clusters can lead during the course of accumulation to a large shift in the frequencies of the betatron oscillations (see Sec. 6, Chapter III). The magnetic system of the storage ring must be so constructed as to keep the frequencies of the betatron oscillations far from the most dangerous resonances. The change in the mean gradient, effected to this end, must not lead to distortion of the equilibrium orbit.

The damping of the longitudinal and transverse oscillations occurs automatically in weak-focusing magnetic systems with $n < 0.75$ [33-36]. However, in strong-focusing systems the radial oscillations experience antidamping due to the faster damping of the longitudinal oscillations [36-39]. Whereas in an accelerator it is possible to tolerate antidamping because of the short

acceleration time, in a storage ring, where the beam exists for a time measured in days, the antidamping is utterly inadmissible. When using strong-focusing systems it is therefore necessary to provide for damping of the radial oscillations (see Sec. 3, Chapter III).

The probability of particle interaction in colliding beams increases with decreasing transverse dimensions of the clusters. The magnetic system of the storage ring must ensure sufficiently small cluster dimensions, since, as was shown above, the cross sections of all expected processes are small.

As follows from estimates that will be given below, the transverse dimensions of the beam are the smaller, the larger the value of $M\nu$ of the betatron oscillations per revolution. A large value of $M\nu$ can be attained in a storage ring only with strong focusing at high values of the magnetic-field gradient. The increase in the number $M\nu$ entails also an increase in the number M (number of periods of the gradient), if the operating point lies in the first stability region. It is usually impossible to go over to a higher stability region, since the permissible deviations of the storage-ring parameters (tolerances) become two orders of magnitude more stringent already in the next region.

In order to place the inflectors, high-frequency resonators, and the physical apparatus in the storage ring it is convenient to have a few straight-line segments as long as possible. In the case when the number of segments is $m < M$, the stability region breaks up into separate bands. The effect of such segments can be regarded as a perturbation of the gradient, and the resultant instability bands are the consequence of parametric resonance. Their positions are determined by the condition for the occurrence of parametric resonance:

$$2M\nu = km, \quad k = 1, 2, 3, \ldots, \frac{M}{m}. \qquad (2.1)$$

Figure 3 shows the occurrence of instability bands for $m = 8$ and $M = 24$.

An increase in the number $M\nu$ is advantageous also from the point of view of the permissible phase space volume of the system. In other words, for equal dimensions of the magnetic-field region, the effective aperture can be made much larger in a strong-focusing system than in a weak-focusing one. The latter circumstance is advantageous from the point of view of injection.

Finally, a rather important distinction between the magnetic system of the storage ring and that of an electron accelerator results from the fact that the magnetic field of the storage ring is constant in time, or varies very slowly. This greatly facilitates the correction of the characteristics of the storage-ring field. The main difficulties of accelerators, namely the presence of low-values of the magnetic field and perturbations introduced by eddy currents are lacking in storage rings. All this makes it possible to stiffen the tolerances of the magnetic-system parameters in

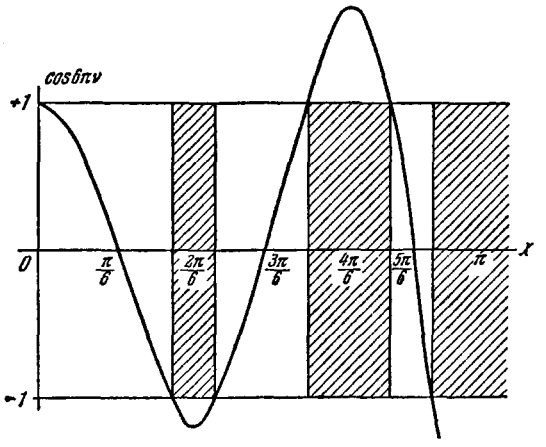

FIG. 3. Stratification of the instability region of betatron oscillations with $m < M$ for the case $M/m = 3$, $\chi = \sqrt{n} l_M/\rho_0$, where ρ_0, l_M, and n are the radius of curvature, length of the magnetic block, and magnetic-field fall-off exponent, respectively.

the storage ring by several times. This makes it possible to choose a more highly stressed variant of the magnetic structure. More stringent tolerances mean a reduction in the possible perturbations for chosen values of the parameters. Both causes reduce further the dimensions of the clusters.

3. High-Frequency System

The high-frequency system of the storage ring is intended for the compensation of the energy lost by the moving particles. These losses are essentially in the form of incoherent synchrotron radiation in the magnetic field.

The presence of radiation is most important to the very possibility of storing the particles. Indeed, according to the Liouville theorem, the phase-space volume occupied by the system does not decrease provided the motion has a Hamiltonian character. This means that for such systems storage can occur only by filling the unoccupied parts of the phase volume, corresponding to stable motion. Such a situation arises, for example, during the storage of protons.

Synchrotron radiation causes the Liouville theorem to break down for electron storage rings, since the motion is not Hamiltonian if the radiation is taken into account. Consequently storage can occur in rings for electrons and positrons by continuous injection of new batches of particles into one and the same phase-space volume, as the latter becomes free of the previously injected particles. The particle density in phase-space increases in this case with continuing storage.

It follows directly that the intensity of the energy losses in the storage ring must be made sufficiently large, so that a sufficiently large part of the volume becomes free during the time between two successive injections.

On the other hand, too high a loss intensity calls

for considerable expenditure of high frequency power for compensation. These two circumstances lead to the existence of an optimal storage-ring radius for a given particle energy and for a given interval between two instants of injection.

The average energy lost per revolution in the form of radiation by an equilibrium particle is given by the formula

$$\frac{\Delta E_{\text{rad}}}{mc^2} = \frac{4\pi}{3}\frac{r_0}{\rho_0}\frac{\lambda_2}{\lambda_1}\left(\frac{E}{mc^2}\right)^4, \qquad (2.2)$$

in which $r_0 = e^2/mc^2$, ρ_0 — radius of curvature of the orbit in a magnetic field H_0, $\lambda_k = \langle H^k/H_0^k \rangle$ — average over the orbit of the field ratio raised to the k-th power.

The amplitude of the high frequency voltage V per revolution in the storage ring is governed principally by the dimensions of the synchrotron-oscillation stability region. For specified amplitude V and specified energy losses ΔE_{rad}, the synchrotron oscillations are executed relative to an equilibrium phase φ_0, defined by the relation $\cos\varphi_0 = \Delta E_{\text{rad}}/eV$. If, as is customarily the case, the injected particles are uniformly distributed over the phases of the high-frequency field and over the energies, then the rate of accumulation is proportional to the area in the phase plane, corresponding to stable motion. We shall assume that the interval of permissible energies is determined by the separatrix. The maximum energy spread is then

$$\left(\frac{\Delta E}{E}\right)_{\text{perm}} = \sqrt{\frac{2eV}{\pi q \alpha E}(\sin\varphi_0 - \varphi_0\cos\varphi_0)}, \qquad (2.3)$$

where q — multiplicity of high frequency and α — logarithmic derivative of the length of the orbit with respect to the momentum.

The permissible phase interval is determined by the equation

$$\sin\varphi + \sin\varphi_0 = (\varphi + \varphi_0)\cos\varphi_0. \qquad (2.4)$$

We see from (2.3) and (2.4) that both the phase interval and the energy interval increase with increasing φ_0. Therefore from the point of view of increasing the rate of accumulation it is convenient to increase the equilibrium phase (or, what is the same, to increase the amplitude of the high frequency voltage for a specified ΔE_{rad}).

We see also from (2.3) that the equilibrium phase (and the voltage amplitude) is smaller in a strong-focusing system than in a weak-focusing system under the same conditions. This is due to the smallness of α for strong-focusing systems.

We now turn to considerations that dictate the choice of the frequency or multiplicity of the electric field. To be specific, let us consider a storage ring for electrons and positrons with a single magnetic track. With a high frequency multiplicity q, there move along the orbit q clusters of particles of each sort. Consequently, the number of points of encounter will be 2q, and their position on the ring is specified by the position of the high-frequency resonators. With the number N of particles in the orbit specified, there are N/q particles in each cluster. Therefore an increase in q reduces the probability of interaction at each point of cluster encounter. It follows from (2.3) that an increase in q decreases $(\Delta E/E)_{\text{perm}}$. All this makes it desirable to decrease q. However, inasmuch as some of the cluster encounter points which are located in the high-frequency resonators are difficult to use for experiments, 2q should be made larger than the number of resonators N_{res}. For example, when q = 2 and $N_{\text{res}} = 2$, there remain two points of cluster encounters available for experiments.

It is also necessary to bear in mind that the high-frequency system of the storage ring must operate continuously for a long time. This imposes special requirements on the reliability of the high-frequency apparatus and greatly increases the required average power of the high-frequency generator. Furthermore, owing to the low multiplicity of the radio frequency, the dimensions of the high-frequency resonator in the storage ring are always much smaller than the wavelength of the electric field. Therefore the Q of the high-frequency intervals cannot readily be made very high.

4. System for the Injection of Particles

The injection of particles into a storage ring is the most difficult practical problem. To capture the particles in the storage mode it is possible either to use special inflector devices or to act on the separatrix[40]. In the latter case the amplitude of the high frequency field is reduced at the instant of injection. This decreases the dimension of the separatrix, but since damping causes the previously accumulated particles to occupy only a small part of the stability region, such a decrease does not affect these particles. The orbits of the injected particles turn in under the influence of the radiation. Once the particles move far away from the "source," the amplitude of the high frequency voltage is restored to its normal value. The damping of the oscillations leads subsequently to a decrease in the oscillation amplitudes, and the process can be repeated.

Another method is to use inflectors and does not differ essentially from injection in an accelerator. However, the high injection energy, the required short time of voltage dip on the inflector, and the presence of the already accumulated particles make the entire problem very difficult. An additional difficulty is that it may be necessary to use two inflectors for the injection of particles moving in opposite directions.

In a storage ring for electrons and positrons, the inflector must be a device with a magnetic field only, since the electric field exerts a different action on the electrons and positrons. Actually, the high injection

energy excludes the possible use of an electric field anyway.

The source of electrons for storage may be an electron accelerator. The positrons intended for storage are obtained by conversion of γ quanta on a target. Different variants of particle injection in a storage ring are possible. In one case the converter target is located outside the storage-ring chamber. In this case charged particles are introduced into the storage-ring chamber. One such injection system, used for the Adone storage ring (Frascati), is shown in Fig. 18. A somewhat different variant, which provides for simultaneous symmetrical injection of electrons and positrons, is shown schematically in Fig. 4. In another case, the converter targets are located directly in the storage-ring chamber (Fig. 5), and one of the components of the produced e^+e^- pairs is captured into the storage mode.

We define the conversion coefficient as the ratio of the number of positrons entering a given solid angle and a given energy interval to the number of primary electrons producing the γ quanta. The conversion coefficient depends on the positron energy, electron energy, thickness t, and material of the targets. In calculating the conversion coefficient account is taken of multiple scattering of the electrons and positrons in the target, the change in the energy spectrum of the positrons due to bremsstrahlung on passage through the target, and absorption of γ quanta in the target. For thick targets ($t > t_{rad}$) the calculation is in accordance with the cascade theory. Both calculation [41] and experiment [42-44] show that the conversion coefficient can be of the order of 10^{-4}, and increases with increasing energy of the stored particles.

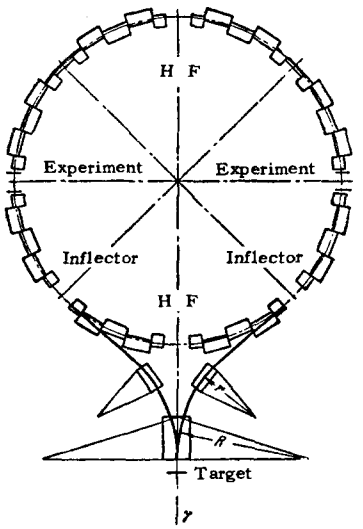

FIG. 4. Symmetrical scheme for the injection of electrons and positrons with external converter target.

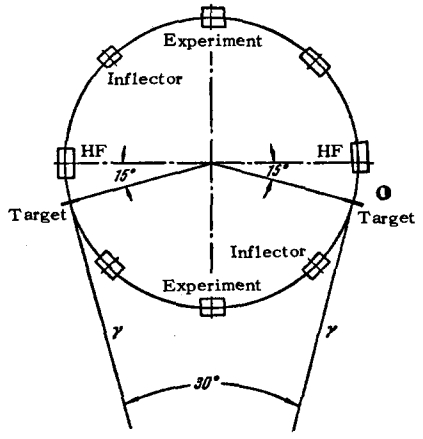

FIG. 5. Possible variant of injection of electrons and positrons from a synchrotron using two internal converter targets.

Each of these injection methods has its advantages. For systems with external converter targets, these advantages are the freedom in mutual placement of the accelerator and storage ring, making it possible to choose the most convenient position for the storage ring, and the control over the beams, since the particles injected in the storage ring are charged.

Furthermore, the system shown in Fig. 4 has the advantage that the number of particles of each sign moving in the storage ring is practically the same. This is preferable from the point of view of the electromagnetic interaction between the clusters (see Sec. 6 of Chapter III) and greatly reduces the loading of the resonator by the beam.*

A shortcoming of this system is the fact that the direct photon beam (and the accompanying particles) travels through the storage ring, and the zones where the experiments are performed are located near the injection points. In the case when the experiment is carried out simultaneously with accumulation of the particles, this may affect adversely the experimental conditions, since it raises the background and scattered-radiation levels.

Advantages of an injection system with two γ beams are the absence of a direct particle beam passing through the storage ring, and also the somewhat greater simplicity of capture of the particles produced in regions with well-known magnetic-field topography. The injection of electrons and positrons from the outside through stray magnetic fields becomes a more difficult problem.

The requirement of symmetry with respect to the positrons and electrons landing on the orbit leads to a symmetrical arrangement of the inflectors. The closed orbit excited by the inflector field must be even with respect to the point situated halfway between the injection places. In this case the probabilities for capturing electrons and positrons are the same. To increase these probabilities, the periodic orbit must have two absolute maxima near the injection locations. If these two maxima are much greater than the maxima at other points of the closed orbit, then the losses of

*For a specified value of the product N_+N_- [see (3.6)] the minimum of the sum $N_+ + N_-$, which determines the beam current, occurs when $N_+ = N_-$.

the particles as they go into orbit will occur predominantly at the injection points.

In the case of simultaneous injection of electrons and positrons the operation of both inflectors must be synchronized to a high accuracy. Alternate operation of the inflectors doubles the storage time and increases the required field intensity in each inflector.

The rate of accumulation of positrons is determined principally by the conversion coefficient. In this sense the strong-focusing system also offers advantages over the weak-focusing one. Indeed, because the effective aperture and the interval of captured-particle energies can be made much greater in the strong-focusing system, the conversion coefficient for such a system is larger.

Thus, an analysis of the requirements imposed on the main units of the storage ring, namely the magnetic, high-frequency, and injection systems, leads to the conclusion that strong-focusing storage rings for high energies have undisputed advantages over weak-focusing storage rings [45]. These advantages are essentially as follows:

1) Lower electric field intensity, and consequently lower power consumption in the electronic part.

2) Smaller transverse beam dimensions and consequently higher reaction rate in the colliding beams.

3) Smaller dimensions of the operating region of the magnetic field for identical effective aperture, and consequently a lighter magnet.

Strong-focusing systems have, however, also disadvantages. Principal among them are:

1) Antidamping of the radial oscillations; this calls for application of damping in one fashion or another, thus complicating the magnetic system.

2) Narrowness of the permissible interval of betatron oscillation frequencies; to increase the rate of accumulation of the particles it is necessary to compensate for the energy dependence of the betatron frequencies [46].

We note also that the partial lifetimes of the beam relative to all processes (except for single inelastic scattering) are longer in a strong-focusing storage ring. However, inasmuch as the total lifetime in a high-energy storage ring is essentially determined precisely by this single inelastic scattering process, this circumstance is not an advantage of strong-focusing storage rings.

III. PROCESSES OCCURRING UPON STORAGE OF ELECTRONS AND POSITRONS

1. Characteristic Motions of Particles in Storage Ring

The motion of the electrons and positrons in a storage ring has precisely the same character as in an accelerator. In this connection, it is convenient to describe this motion using the techniques developed for the design of accelerators. Some difference results only from the interaction between the clusters.

The magnetic part of the Lorentz force is invariant under reversal of the sign of the charge with simultaneous reversal of the sign of the particle velocity. Consequently, the trajectories of the positron and of the electron that moves opposite to it coincide under suitable initial conditions in a magnetic field of any configuration.

It is convenient to study the motion of aggregates of particles moving in each direction relative to a closed orbit that is common to all particles of the given group. All possible free oscillations, corresponding to the distribution of particles by initial deviations and velocities, are reckoned from this orbit. If the free oscillations in all the coordinates are damped, then in the final analysis the two aggregates of particles in each group can be characterized by two closed orbits, to which the free oscillations collapse.

Real closed orbits are determined completely by the magnetic and electric fields with all the existing perturbations (including those produced by the beams themselves) and do not depend on the initial conditions, provided the external field does not contain any nonlinear terms.

The electrical part of the Lorentz force reverses sign with reversal of the charge sign. Therefore the electrical components which are transverse relative to the direction of motion can lead to the divergence of the closed orbits. The longitudinal component of the electric field leads to a change in the particle energy

$$\frac{dE}{dt} = e\mathbf{E}\mathbf{v}. \qquad (3.1)$$

Inasmuch as the right side of (3.1) contains the product of the charge and the velocity, the positron and the electron moving opposite to it are accelerated by the same electrical field.

The motion of the electron (and positron) in a magnetic field is accompanied by radiation of energy. For high-energy particles this circumstance determines the entire dynamics of particle motion in the storage ring. Because of radiation, the particle motion is not Hamiltonian. In particular, for such a motion the Liouville theorem is violated, and this, properly speaking, makes storage possible.

In order for the trajectory of the particle to remain constant in a constant magnetic field, it is necessary to compensate for the average energy losses by means of the high-frequency electric field. This leads in turn to radiative damping (or antidamping) of the oscillations. The total volume of the phase space occupied by the particles decreases, and it can be replenished continuously with new particles, thereby effecting their storage. The limit of such storage arises theoretically only because of the interaction between the particles themselves.

The fluctuations of the radiation (and also other factors) cause oscillations to build up. As a result of

simultaneous action of buildup and damping, the oscillations reach stationary amplitudes that determine the dimensions of the clusters of stored particles.

At the same time, these factors lead also to the loss of particles and to a finite lifetime in the storage ring. The lifetime is quite negligible in the presence of antidamping in even one degree of freedom. Consequently, the storage ring must be constructed such that the oscillations are damped in all degrees of freedom.

Depending on the parameters of the storage ring and on the accelerator beam intensity, two operating modes of the storage ring are possible. If the accumulation to the maximum current is rapid compared with the lifetime of the beam in the storage ring, then the accelerator is either turned off after the limiting current is reached, or else is switched over to other experiments. The experiments in the storage ring are performed on the accumulated beams. On the other hand, if the lifetime of the beam is comparable with or shorter than the accumulation time, then the accumulation and the experiment are carried out simultaneously. The accelerator is used all the time to feed the storage ring.

2. Probability of Particle Interaction in Colliding Beams

Let us obtain estimates for the probability of particle interaction in colliding beams[47]. We assume for simplicity that the density of the particles is constant over the cross section of the cluster. We consider first the collision of two identical particle clusters moving opposite each other with velocities v_1 and v_2 in the laboratory frame.

Let us assume that the length l_0 of the interaction region, i.e., the region within which events are recorded by the apparatus, is much smaller than the length d_φ of the clusters. The time that it takes for the particle to pass through the interaction region is l_0/v_1. During that time there enter into the interaction region also particles of the second cluster, which are located at a distance not larger than $l_0 v_2/v_1$.

The effective interaction length is thus equal to $l_0(1 + v_2/v_1)$. The probability of interaction of one particle with the second cluster over a length l_0 is equal to

$$W = n_2 \sigma l_0 \left(1 + \frac{v_2}{v_1}\right), \tag{3.2}$$

where n_2 —density of the particles in the second cluster, σ —effective cross section of interaction. The probability of interaction for all N_1' particles of the first cluster is

$$W = N_1' n_2 \sigma l_0 \left(1 + \frac{v_2}{v_1}\right). \tag{3.3}$$

Thus, in one collision of two clusters, the probability of any process with cross section σ, registered over an interaction length l_0, is equal to

$$W' = 2N_1' N_2' \frac{\sigma}{S} \frac{l_0}{d_\varphi}, \tag{3.4}$$

where N_1' and N_2' are the numbers of the particles in each cluster and S is the cross section of the cluster. The probability per second, W_1, can be obtained by multiplying W′ by the number of cluster collisions per second. When the clusters travel on a closed trajectory, the number of collisions at one point of the orbit is equal to the frequency of the electric field q/T, where T is the period of revolution of the clusters. If we take N_1 and N_2 to mean the total number of particles on the orbit, then

$$W_1 = \frac{2N_1 N_2}{STq} \sigma \frac{l_0}{d_\varphi}. \tag{3.5}$$

To increase the accuracy of the experiment, the interaction region l_0 should be made as small as possible. This, and also a few other considerations, make it necessary to effect crossing of the beams inclined at a small angle $\delta \ll 1$ rad to the direction of motion. Denoting the length, width, and height of the clusters by d_φ, d_r, and d_z, respectively, we obtain

$$W_1 = \frac{2N_1 N_2 \sigma}{Tq\delta d_\varphi d_r} = R\sigma. \tag{3.6}$$

The coefficient R in this formula is called the "transmission."

3. Damping of Oscillations

The presence of radiation gives rise to a specific radiative damping, which decreases the phase-space volume occupied by the cluster. The damping of the oscillations in the storage ring is characterized by a time τ_d, during which the square of the oscillation amplitude decreases by a factor e.

For vertical oscillations, not connected with other oscillations of particles, this time is equal to

$$\tau_z = \frac{E}{W_0}\lambda_2^{-1} = \frac{E}{\Delta E_{\text{rad}}} T, \tag{3.7}$$

where ΔE_{rad} is the energy radiated over the time T of one revolution of the particle, W_0 is the radiation power in a magnetic field H_0, and $\lambda_2 = \langle H^2/H_0^2 \rangle$. The corresponding times for the radial and phase oscillations are

$$\tau_r = \beta_r^{-1} \frac{E}{W_0}, \tag{3.8}$$

$$\tau_\varphi = \beta_\varphi^{-1} \frac{E}{W_0}. \tag{3.9}$$

The coefficients β_r and β_φ depend on the structure of the magnetic field and are connected by the relation $\beta_r + \beta_\varphi = 3\lambda_2$. The coefficient β_φ is defined by the formula[48,49]

$$\beta_\varphi = \left[2 - \left\langle (2n-1)\frac{\psi}{\rho} \right\rangle\right] \lambda_2, \tag{3.10}$$

where ρ is the radius of curvature and $\psi(\theta)$ is a function that describes the periodic orbit connected with the deviation of the particle energy from the equilibrium value. Using the equation for $\psi(\theta)$, we can reduce this expression to the following form[48]:

$$\beta_\varphi = \lambda_2(2-\alpha) + 2\lambda_1 - 2\left\langle (n-1)\frac{\varrho_0^2}{\varrho^2}\frac{H-H_0}{H_0}\frac{\psi}{\varrho_0}\right\rangle, \quad (3.11)$$

where $\lambda_k = \langle H^k/H_0^k\rangle$ and the subscript 0 designates all the quantities that are taken as standards. In a weak-focusing storage ring we have

$$\alpha = \frac{1}{1-n}, \quad \lambda_2 = \lambda_1, \quad \beta_\varphi = \frac{3-4n}{1-n}\lambda_2, \quad \beta_r = \frac{n}{1-n}\lambda_2,$$

that is, when $n < 0.75$ both the phase and radial oscillations are damped. In a strong-focusing storage ring without damping we have

$$H = H_0, \quad \alpha \ll 1, \quad \beta_\varphi = 2(\lambda_2 + \lambda_1) > 0, \quad \beta_r = -2\lambda_1 + \lambda_2 < 0,$$

that is, the radial oscillations experience antidamping [36]. Because of this, the strong-focusing storage ring without damping loses the beam after a very short time.

Several methods of damping the oscillations are possible [49-53]. One convenient method for damping radial oscillations is to reduce the magnetic field in the magnets that focus with respect to r, compared with the field of the defocusing magnets. From the formulas obtained in [48] we readily obtain the following estimate for the relative field difference:

$$\frac{H_D - H_F}{H_D} = 1 - \frac{\int_{n>0}\psi\, d\theta}{\int_{n<0}\psi\, d\theta}. \quad (3.12)$$

Formula (3.12) has been obtained under the assumption that the damping is produced in such a way that the focusing properties of the system do not change, that is, the gradients, which are the same in both magnets, remain the same, as do the lengths. The decrease in the field in the focusing blocks leads to an increase in the radius of curvature and to a decrease in the distance to the neutral pole in these blocks.

Another method of damping the oscillations is used in the design of the Adone storage ring (see Sec. 3 of Chapter IV).

We shall assume henceforth that the system ensures damping of all types of oscillations, so that $\beta_r > 0$ and $\beta_\varphi > 0$. The largest among the times τ_d determines the time interval between two successive injections of particles in the storage ring. This interval must satisfy the inequality $\Delta t > \tau_d$.

The time interval Δt determines the maximum number of particles which can be stored in a given apparatus. If ΔN particles are captured in the storage ring during each injection, then the steady-state number of particles is determined by the relation

$$N = \frac{\tau_{eff}}{\Delta t}\Delta N, \quad (3.13)$$

where τ_{eff} — effective lifetime of the beam (time during which the number of particles decreases by the factor e in the absence of injection).

4. Particle Losses and Lifetime of Beams in Storage Rings

There are many reasons for the loss of particles in a storage ring. All can be regarded as independent. If we introduce for each of the reasons a partial lifetime τ_i, then the effective lifetime is determined from the formula

$$\tau_{eff} = \left(\sum_i \frac{1}{\tau_i}\right)^{-1}. \quad (3.14)$$

The main reasons for the loss of particles in a storage ring are the following:

1. Bremsstrahlung. The emission of a photon with energy $\Delta E > (\Delta E)_{perm}$, where $(\Delta E)_{perm}$ — width of the separatrix, occurring upon collision between the electrons and the atoms of the residual gas, causes the particle to drop out of the region of stable longitudinal motion. The particle gradually loses its energy (by synchrotron radiation), and its trajectory swings away until the particle is lost on the vacuum-chamber wall. The lifetime with respect to this process is [54]

$$\tau_{br} = \frac{6.5\cdot 10^{-2}}{Z^2 p \ln\frac{E}{(\Delta E)_{perm}}} \approx \frac{2.7\cdot 10^{-4}}{p} \text{ sec}. \quad (3.15)$$

Here p — pressure (in mm Hg) of the residual gas of atomic number Z. We see that the time τ_{br} is practically independent of any other parameters of the storage ring. In order for the beam to exist for a time longer than 3×10^5 sec, the pressure in the chamber cannot exceed 10^{-9} mm Hg.

We note incidentally that the electron beam is a potential well for the positive ions of the residual gas. Therefore the pressure in the region of motion of the beam can differ noticeably from the pressure in the rest of the chamber. To eliminate this effect, the storage ring must be provided with a clearing electric field. The clearing electrodes must be so constructed as to perturb as little as possible the motion of the particles in the storage ring [84]. To this end, the clearing electric field must reverse its sign along the equilibrium trajectory sufficiently often.

2. Single Coulomb scattering. Let us consider first the collision between particles inside a cluster. [87] In such a collision the particle can acquire an additional longitudinal momentum which is large enough to bring it outside the synchrotron-oscillation stability region. The lifetime of the beam with respect to this effect is proportional to $E^{9/2}$, and in the presence of a radial-vertical coupling between the oscillations even to $E^{11/2}$. This is precisely the character of the beam lifetime observed experimentally in the AdA installation [87].

In elastic scattering by the atoms of the residual gas, the particle is lost by collision with the chamber wall (which is essentially horizontal), if the scattering angle exceeds $\theta_{min} \approx 4b_z M\nu_z/L$, where $M\nu_z$ is the number of vertical betatron oscillations along the length L of the orbit and b_z is half the chamber height. The lifetime with respect to this process is [54]

$$\tau_{sc} = \frac{4.7\cdot 10^{-4}\theta_{min}^2}{Z^2 P}\left(\frac{E}{mc^2}\right)^2 \text{ sec}; \quad (3.16)$$

τ_{sc} increases like $(E/cm^2)^2$, and for a specified an-

gular aperture of the chamber (b_z/L) it is proportional to $(M\nu_z)^2$.

3. Fluctuations of radiation. This process leads to a stochastic increase in the beam dimensions [35-39,61-66] and consequently to loss of particles. The damping of the oscillations hinders the increase in the dimensions, so that the joint action of damping and fluctuations leads to establishment of equilibrium time-independent mean-square oscillation amplitudes. The mean-square amplitude of the radial oscillations is determined by the expression [55]

$$\overline{A_r^2}_{\text{free}} = 2.68\cdot 10^3 \frac{|\Phi_r|^2_{\max}\left|\left\langle \frac{\varrho_0}{\varrho}\Phi_r\right\rangle\right|^2 \lambda_3 r_0 \varrho_0}{M^4 \sin^2(\pi M\nu_r)\cdot\lambda_1^4\beta_r}\left(\frac{E}{mc^2}\right)^2. \quad (3.17)$$

Analogous expressions for the radial-phase and phase oscillations are:

$$\overline{A_r^2}_{\text{forced}} = 1.34\cdot 10^3 \frac{|\Phi_r|^2_{\max}\left|\left\langle \frac{\varrho_0}{\varrho}\Phi_r\right\rangle\right|^2 \lambda_3 r_0 \varrho_0}{M^4 \sin^2(\pi M\nu_r)\cdot\lambda_1^4\beta_\varphi}\left(\frac{E}{mc^2}\right)^2, \quad (3.18)$$

$$\overline{A_\varphi^2} = 4.08\cdot 10^2 \frac{\lambda_3\lambda_1}{\lambda_2\beta_\varphi}\frac{q\alpha}{\operatorname{tg}\varphi_0}\frac{mc^2}{E}. \quad (3.19)^*$$

In these formulas Φ is the Floquet function, normalized by the condition

$$\frac{\Phi\, d\Phi^*}{d\theta} - \frac{\Phi^*\, d\Phi}{d\theta} = -2i.$$

Radiation fluctuations lead also to a buildup of vertical betatron oscillations, if we take account of the fact that the quantum can be emitted at an angle to the direction of the velocity of the moving particle. This angle has an order of magnitude (mc^2/E). This effect occurs also for radial oscillations, but for the latter it is only a small addition to the main effect. For vertical oscillations, on the other hand, only with account of this effect does fluctuation of radiation lead to buildup of oscillations [36-39,52,56]. The mean-square amplitude of the vertical oscillations is determined by the formula

$$\overline{A_z^2} = \frac{13\sqrt{3}}{48}\frac{\hbar}{mc}|\Phi_z|^2_{\max}\overline{|\Phi_z|^2}\frac{\lambda_1}{\lambda_2}\varrho_0. \quad (3.20)$$

The lifetime of the beam is a function of the ratio $\xi = A^2_{\text{perm}}/\overline{A^2}$, where A_{perm} is the dimension of the corresponding region of stability of oscillations. When $\xi \gg 1$ it is determined by the formula [57,58]

$$\tau_{\text{rad}} = [\overline{Ei}(\xi) - \ln\xi - 0.577]\,\tau_d, \quad (3.21)$$

where $\overline{Ei}$ is the integral exponential function [68]. In order for the lifetime due to fluctuations to be of the order of 3×10^5 sec (with $\tau_d \approx 10^{-2}$ sec), the inequality $\xi \gtrsim 30$ must be satisfied.

For radial and radial-phase oscillations it is possible to attain this inequality by increasing the radial dimensions of the vacuum chamber and the working region of the magnetic field. For phase oscillations it is necessary to increase φ_0 and to reduce the high-frequency multiplicity. It is seen from (3.19) that owing to the smallness of α it is easier to obtain a large lifetime (relative to the process under consideration) in a strong-focusing system than in a weak-focusing system. For vertical oscillations, the required inequality is certainly satisfied, in view of the smallness of the mean-square amplitudes $\overline{A_z^2}$.

For $\xi \sim 1$ Formula (3.21) loses its validity. The lifetime can be determined under these conditions from the formulas and plots of [57].

4. Multiple Coulomb scattering by atoms of the residual gas. Multiple scattering leads to a stochastic buildup of betatron oscillations (radial and vertical). The steady-state mean-square amplitude due to the scattering can be estimated from the formula [54]

$$\overline{A^2_{r,z}} = 3.64\cdot 10^5 \frac{Z^2 P\,|\Phi_{r,z}|^2_{\max}\overline{|\Phi_{r,z}|^2}}{\beta_{r,z}M^2\lambda_1^2}\varrho_0^4\Lambda\left(\frac{mc^2}{E}\right)^5 \text{cm}^2, \quad (3.22)$$

where M — number of periods of the gradient and Λ — Coulomb logarithm.

Particle losses (and a reduction in the lifetime) can also be caused by other factors that increase the amplitudes of particle oscillation (noise in the frequency and voltage of the electric field, passage through shallow nonlinear resonances, etc.).

We note that the formulas of the present section can be used also for a weak-focusing storage ring. To this end the quantity $|\Phi|^2_{\max}\overline{|\Phi|^2}(\rho_0/\lambda_1 M)^2$, wherever it appears, must be replaced by ρ^2/k, where $k = n$ for vertical oscillations and $k = 1-n$ for radial oscillations.

5. Estimates of Cluster Dimensions

Cluster dimensions play an important role in the choice of the storage-ring parameters, for along with the injection requirements they determine the necessary dimensions of the working region of the magnetic field and the reaction rates in the colliding beams.

The formulas of the preceding section make it possible to estimate the cluster dimensions. We mean by cluster dimension double the steady-state root-mean-square amplitude of the oscillations, $2\sqrt{\overline{A^2}}$.

The vertical dimension of the cluster is determined essentially by two effects. First, radiation fluctuations. The vertical dimension of the cluster due to this factor can be determined from (3.20). Second, scatter in the frequencies of the betatron oscillations of the particles, due to the energy dependence of the frequency, can also lead to a broadening of the beam. Indeed, if resonant perturbations are present in the magnetic system and lead to an increase in the oscillation amplitude, then the increment in the amplitude depends on the difference $M\epsilon$ between the oscillation frequency and the resonance frequency. For example, for random deviations of the magnetic field from block to block, the additional broadening of the beam due to the frequency scatter $\Delta M\nu_z$ is

*tg = tan.

$$\Delta d_z = |\Phi_z|_{\max} \frac{\left(\frac{l}{2\pi}\right)^2}{2\varrho_0 M\varepsilon} \sqrt{2M} \sqrt{\sum_{k=1}^{M} \frac{(H_k - H_0)^2}{MH_0^2}} \left| \left\langle \frac{\varrho_0}{\varrho} \Phi_z \right\rangle \right| \Delta M v_z. \quad (3.23)$$

The cross section of the beam at the point of collision should be as small as possible. Therefore, and also because of the tendency to increase the energy region of particle capture, it is necessary to compensate for the dependence of the betatron frequencies on the energy. Multiple Coulomb scattering in the storage ring of electrons plays apparently a secondary role [59].

The radial dimensions of the cluster are determined by the quantum radiation fluctuations. The increase in the radial dimension due to multiple scattering, which has the same order of magnitude as for the vertical oscillations, can be neglected. To determine the radial dimension it is necessary to take into account both free and forced oscillations: $d_r = 2\sqrt{\overline{A^2_{r.free}} + \overline{A^2_{r.forced}}}$.

Finally, the longitudinal cluster dimension is also determined by the quantum radiation fluctuations. The length of the cluster in degrees of the electric field can be calculated from (3.19). The linear length of the cluster is

$$d_\varphi = \frac{L}{q} \cdot \frac{2\sqrt{\overline{A^2_\varphi}}}{2\pi}. \quad (3.24)$$

Finally, the energy scatter of the particles in the cluster is determined by the formula

$$\overline{\left(\frac{\Delta E}{E}\right)^2} = \frac{1}{2}\left(\frac{\Omega}{q\omega\alpha}\right)^2 \overline{A^2_\varphi}, \quad (3.25)$$

where Ω and ω are the frequencies of the phase oscillations and of the revolution, respectively.

The product $d_r d_z = S$ at the point of collision determines the rate of the reactions in the colliding beams. The quantities d_r and d_z at the point of collision are determined from the same formulas (3.17), (3.18), and (3.20), except that $|\Phi|^2_{\max}$ must be replaced by $|\Phi|^2$ at the point of collision of the beams.

Formulas (3.17) and (3.18) illustrate the already mentioned fact that the transverse cluster dimensions, and consequently, the reaction rates in a strong-focusing storage ring are higher than in a weak-focusing ring.

We note also that the cluster dimensions in the storage ring satisfy the strong inequalities

$$d_z \ll d_r \ll d_\varphi, \quad (3.26)$$

so that the particle clusters are reminiscent of long and broad ribbons.

6. Electromagnetic Interaction Between Clusters in a Storage Ring

We proceed now to effects that limit the current of the accumulated particles. Principal among them is the electromagnetic interaction between clusters [45,67,69].

Electromagnetic interaction between particles occurs also in accelerators, but there its magnitude is much smaller, since the electric repulsion between the charges in the cluster is almost completely compensated in the case of ultrarelativistic particles by the magnetic attraction between them.

The interaction between particles belonging to the same cluster has in storage rings a similar character, but we have here in addition the interaction between particles belonging to two different colliding clusters. The electric and magnetic forces of such an interaction are additive. In a storage ring for electrons there is added to the electric repulsion of like charges also the magnetic repulsion of the opposing currents. In a storage ring for electrons and positrons, the electric attraction of unlike charges adds up with the magnetic attraction of currents flowing in the same direction. This interaction causes a shift in the betatron frequencies and a divergence of the equilibrium orbits of particles moving in opposite directions. When the particle density in the clusters is sufficiently high, the divergence of the orbits may exceed the transverse dimensions of the clusters, so that the latter cease to collide at all.

Let us consider both effects using as an example a storage ring for electrons and positrons. We assume for simplicity that the clusters are in the form of flat ribbons, the dimensions of which in height, width, and length satisfy the inequalities (3.26). The charge distribution inside the cluster will be assumed uniform. These assumptions are apparently not too far from reality. Figures 6 and 7 show schematically the vertical components of the force $f_z(z)$ exerted on the particle by the oppositely moving cluster, for two different mutual positions of the clusters at the point of encounter—for clusters that have diverged apart in the vertical direction and for those that overlap completely. Those are the two extreme cases.

From the character of the dependence of the function $f_z(z)$ it follows that for clusters that have diverged apart the correction to the betatron frequency

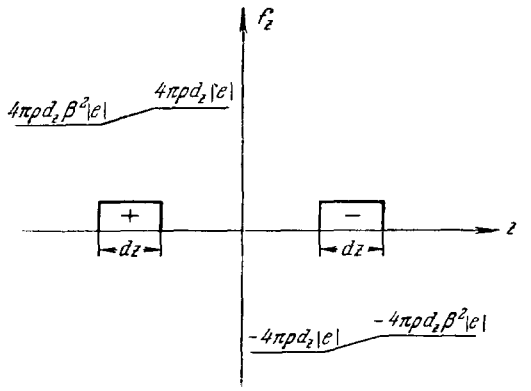

FIG. 6. Vertical components of the forces f_z, acting on the electrons and positrons, for clusters that have diverged apart in a vertical plane.

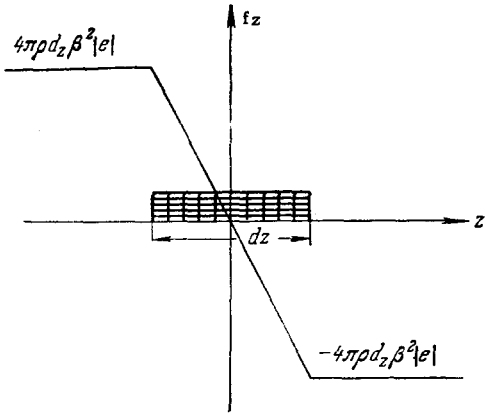

FIG. 7. Vertical component of the force $f_z(z)$, acting on a particle, for completely overlapping clusters.

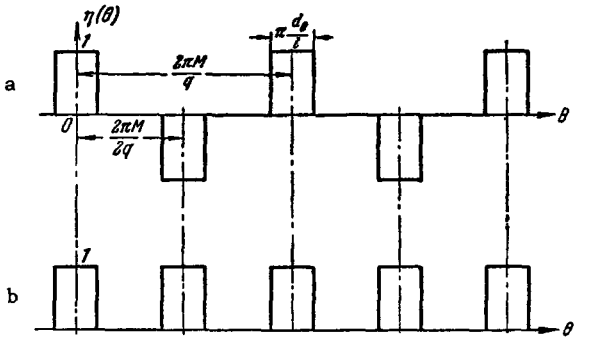

FIG. 8. Periodic function $\eta(\theta)$ which takes into account the mutual position of the electron and positron clusters at the instants of encounter.

contains an additional factor $(mc/p)^2$ and can be neglected. This is due to the weak dependence of $f_z(z)$, connected only with the difference between β^2 and unity. The principal effect consists in a distortion of the equilibrium orbit of the clusters.

Let us assume that the clusters are separated at the point of encounter by a distance larger than the height of the cluster. It is easy to obtain an expression for the force acting on a particle in one of the clusters (say the first) due to the other ($\beta = 1$):

$$f_z = 4\pi \frac{N_2 |e| e}{d_\varphi d_r q} \eta(\theta). \qquad (3.27)$$

The function $\eta(\theta)$ characterizes the dependence of the interaction force on the azimuth θ. Owing to the periodicity of the cluster encounters, $\eta(\theta)$ is a periodic function of θ.

The length of the period of the function $\eta(\theta)$ depends on the character of the equilibrium orbits of the clusters. Figure 8 shows the function $\eta(\theta)$ for two possible periodic orbits. In case a) the clusters interchange places after each encounter (in the sense of deflection from the central plane). In case b) the clusters pass through the points of encounter always on one side of the central plane.

The periodic force $f_z(\theta)$ gives rise to a new equilibrium orbit $z(\theta)$. For the function $\eta(\theta)$ shown in Fig. 8a, the value of z at the point of cluster encounter is found to be

$$z_1 = -\frac{N_2 |e| e}{2Eq} \frac{l}{d_r} |\Phi_z|^2 \operatorname{tg} \frac{\pi M \nu_z}{2q}, \qquad (3.28)$$

where l = L/m is the length of the period of the magnetic system. For the function $\eta(\theta)$ shown in Fig. 8b we have

$$z_1 = \frac{N_2 |e| e}{2Eq} \frac{l}{d_r} |\Phi_z|^2 \operatorname{ctg} \frac{\pi M \nu_z}{2q}. \qquad (3.29)^*$$

An analysis of the obtained expressions shows that only one of them corresponds to a stable periodic orbit. Namely, if $\tan(\pi M\nu_z/2q) > 0$, then the deflection (3.28) corresponds to a stable periodic orbit and (3.29) to an unstable one, and vice versa.

The distance between clusters at the point of encounter is equal to $z_1 + z_2$. From the condition $z_1 + z_2 < d_z$ we can determine the limiting number of particles, at which collisions are still possible. For the case $N_1 = N_2 = N$ we have

$$N_{\text{crit}} = \frac{Eqd_r d_z}{e^2 l |\Phi_z|^2} \begin{cases} \operatorname{ctg} \frac{\pi M \nu_z}{2q}, & \text{if } \operatorname{tg} \frac{\pi M \nu_z}{2q} > 0, \\ -\operatorname{tg} \frac{\pi M \nu_z}{2q}, & \text{if } \operatorname{tg} \frac{\pi M \nu_z}{2q} < 0. \end{cases} \qquad (3.30)$$

We note that the value of the divergence or of the limiting current depends on which of the two possible orbits is stable. For a correct choice of the relation between $M\nu_z$ and q, the limiting current may turn out to be one order of magnitude higher. A formula analogous to (3.30) was first obtained in [69] for a weak-focusing storage ring.

The study of equilibrium orbits having different periodicities (for example, a periodicity equal to 2, 3, etc., distances between points of encounter) leads to the deduction that the clusters can be further stratified in the vertical plane [70], since a large number of stable equilibrium orbits is produced.

Let us assume now that the clusters overlap during the time of encounter. The principal effect in this case is the frequency shift of the vertical oscillations. The vertical component of the force is equal to in this case (see Fig. 7)

$$f_z = -8\pi \frac{N_2 e^2}{d_\varphi d_r d_z q} z \eta(\theta). \qquad (3.31)$$

In this case the function $\eta(\theta)$ corresponds to Fig. 8b. From this we obtain for the frequency shift

$$\Delta M\nu_z = \frac{N_2 e^2 M l}{\pi d_r d_z E q} |\Phi_z|^2. \qquad (3.32)$$

If no measures are taken to compensate for this effect, then it is possible to determine from this also the limiting number of particles for which the motion is still stable. By specifying the permissible frequency shift $(\Delta M\nu_z)_{\text{perm}}$ (this can be equal, for example, to the distance to the nearest resonance), we readily obtain

*ctg = cot.

$$N_{2\,\mathrm{lim}} = \frac{\pi d_r d_z q E (\Delta M \nu_z)_{\mathrm{perm}}}{e^2 M l}. \qquad (3.33)$$

The frequency shift in the case of overlapping clusters occurs in the same direction for particles belonging to both clusters. In a storage ring for electrons and positrons, the frequencies of the vertical betatron oscillations increase, while in a storage ring for electrons they decrease. The shift for a given cluster is proportional to the number of particles in the other cluster. Because of this, the frequency shifts in the case of currents of different magnitude are different, and they cannot be compensated for with quadrupole lenses. It can therefore be thought that the accumulation of equal currents can be carried out to appreciably greater values than the accumulation of beams of different intensity.

The orbit divergence considered above can be used for the accumulation of large currents, for the phase shift becomes perfectly negligible following the orbit divergence. The current density is limited in this case only by the interaction of the particles inside the cluster, which is of order $(mc/p)^2$ relative to the interaction of the colliding clusters.

IV. STRUCTURAL FEATURES OF STORAGE RINGS

Modern accelerator technology affords rather modest experience in the construction of storage rings. Many problems involving the principles and the engineering of storage rings have not yet been experimentally verified. The very process of interaction between two beams of appreciable intensity calls for a deep study. Nonetheless, we can point already at several interesting design solutions.

The present chapter is devoted to a review of the designs of several storage rings now under construction.

1. Stanford Electron Storage Ring

The storage ring of Stanford University, for two electron beams at 500 MeV energy, is one of the first projects of experimentation with colliding beams [71-74].

Figure 9 shows a general diagram of the installation (a) and a section through the magnet (b). The magnet comprises a system of two rings, with four sectors in each. At a radius of curvature of 1.4 m, the magnetic field on the equilibrium orbit is 12 kOe.

The electron beams in each of the rings move clockwise in plan. The straight-line section which is common to both rings is where the beams interact.

All the sectors of the magnet have identical structure. Inasmuch as the trajectories of the two beams are quite close in the sections of the electromagnet adjacent to the common straight-line section, it is impossible to ensure in these sections, for each of the beams, the same sign of the gradient as in the entire ring. Therefore the magnetic field is assumed homogeneous (n = 0) [74] at a distance of 38 centimeters

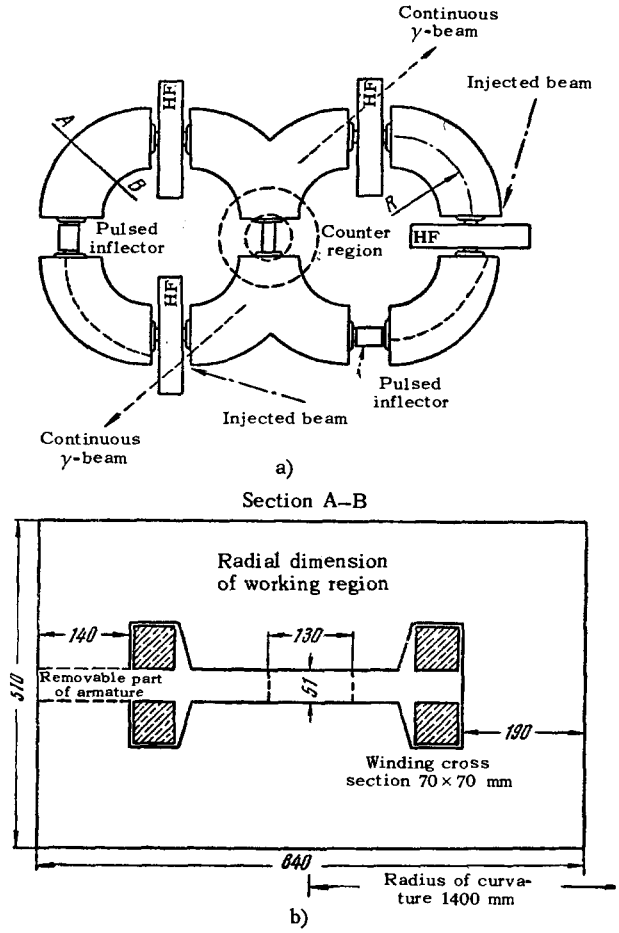

FIG. 9. Diagram of the Stanford electron storage ring.

from each edge of the sector, with the magnetic track having a width of 15 cm. The central part of the sector has n = +1.05. The total weight of the electromagnet is 46 tons.

Each ring has two resonators with Q = 5000, operating at 25.8 Mc. The resonator voltage amplitude is 40 kV.

The injector of the storage ring is a linear accelerator, which produces a current pulse of 8 mA in an energy interval $\Delta E/E = \pm 0.5\%$. The duration of the pulse can be made approximately 100 nsec at a repetition rate of 60 per second. The injected beam is guided to the particular ring by a system of electromagnets.

Before becoming captured in the storage mode, the injected electrons pass through one sector of the electromagnet outside the region of motion of the circulating beam (Fig. 10). At that they move approximately one-half of the path along the magnetic channel, and then, after covering a certain path in the gap of the electromagnet, they enter the pulsed inflector.

The inflector is a pulsed ferrite magnet, separated in length into three sections of 10 centimeters each, fed in parallel. The pulse at the input of the single-turn winding of the inflector is 25 kV. These pulses produce in the inflector winding a current of 2500 A,

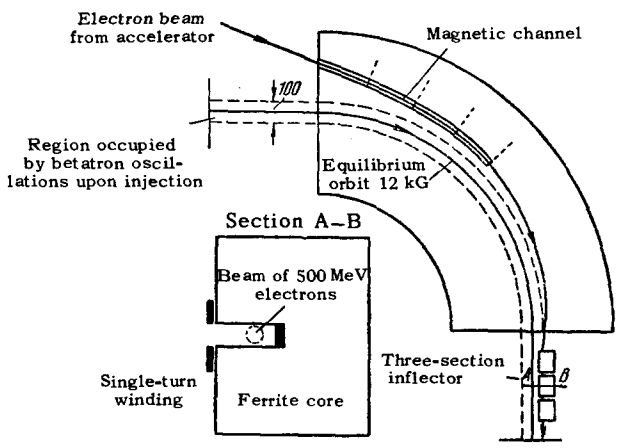

FIG. 10. Diagram showing injection of electrons in the Stanford storage ring.

ensuring a magnetic field of 3100 Oe in the inflector gap. Such a magnetic field deflects the electrons by an angle of 0.06 radian. The injection can last for not more than 4 revolutions, for after the fourth revolution the beam approaches the inflector gap and there should be no magnetic field in the gap in this case. Accordingly, the duration of the inflector pulse is 60 nsec, with a front rise time of ~ 50 nsec.

According to theoretical calculations, the azimuthal, radial, and vertical dimensions of the stored beam are 60 cm, 5 mm, and a few tens of microns, respectively. To attain a "transmission" $R \approx 3 \times 10^{30}$ cm^{-2} sec^{-1} [see (3.6)] for the foregoing beam dimensions, it is necessary to have in each ring a circulating current ~ 1.5 A.

In view of the fact that the limiting current, due to the electromagnetic interaction between the clusters (see Sec. 6 of Chapter III), is much smaller than this value, provision is made in the Stanford storage ring for the beams to cross at a small angle in the vertical plane. To this end magnets are installed on the edges of the common straight-line section; they produce a radial magnetic field H = 4000 Oe over a length of 10 centimeters. Under the influence of these magnets, the beam crosses at the point of encounter at an angle $\delta \approx 0.03$ rad. The maximum shift of the orbit from the central plane is in this case ~ 5 mm.

Owing to the crossing of the beams, the efficiency of their interaction does not depend on the vertical dimension of the beam, and the region of interaction is localized within several centimeters in azimuth.

The average expected lifetime of the beam at a vacuum of 10^{-9} mm. Hg is on the order of 30 hours.

Provision is made for using approximately 100 counters in experiments on the scattering of electrons by electrons. The counters are mounted on a spherical surface of 30 cm radius about the center of the straight-line section, with the exception of the places where the chamber or the magnet prevent their installation. Each pair of counters placed symmetrically about the center of the straight-line section is connected for coincidence. Inasmuch as in elastic scattering the electrons are emitted in opposite directions, this method of connection makes it possible to reduce greatly the noise/effect ratio. Further improvement in this ratio can be attained by limiting the energy interval of the detected particles, since the scattered electrons have the same energy as the incident ones (except for cases with emission of γ quanta).

The total number of registered scattering events expected in the Stanford storage ring is ~ 3 events/sec.

Another possibility of using the storage ring is to obtain continuous γ beams (see Fig. 9) by multiple passage of the stored particles through a thin or gaseous target. To extract these beams from the storage ring, the armature of the magnet is provided with a removable part.

The main parameters of the storage ring are given in the summary table VI[75].

2. Storage Ring of the Frascati National Laboratory (AdA)

The AdA storage ring (anello di accumulazione) for an energy of 250 MeV was constructed in order to study the accumulation process[76]. Tests of the storage ring have shown that the installation can be used also for physical experiments.

The AdA magnet (Fig. 11) consists of a central core 2, an upper and lower armature 1, and pole pieces 4, which produce in the gap a fall-off of the magnetic field with n = 0.6. The pole pieces form four quadrants of 90° each, separated by "straight-line" gaps 18 centimeters each. The height of the gap between the pole pieces amounts to 5.0 cm. The nominal value of the magnetic field in the gap is approximately 14000 Oe. The "straight-line" gaps are not completely free of the magnetic field, but have only an increased gap, equal to the distance between the upper and lower armature.

In the gap of the electromagnet is located a vacuum chamber (Fig. 12), made of stainless steel 1.2 millimeters thick. The curvilinear parts of the chamber are made by stamping the upper and lower walls with subsequent argon-arc welding along the outside and inside radii of the chamber. The obtained curvilinear section was electrically polished with electrolyte E262 provided by the Delmet Milano company. After termination of the electric polishing, all the units of the chamber were welded, including the resonator, target, etc. The assembled chamber was completely evacuated by a diffusion pump with a nitrogen trap, to a pressure on the order of 1×10^{-6} mm Hg. During the course of this evacuation, which lasted for about four days, the chamber and all the units mounted on it were heated to a temperature t = 400° C. The chamber was

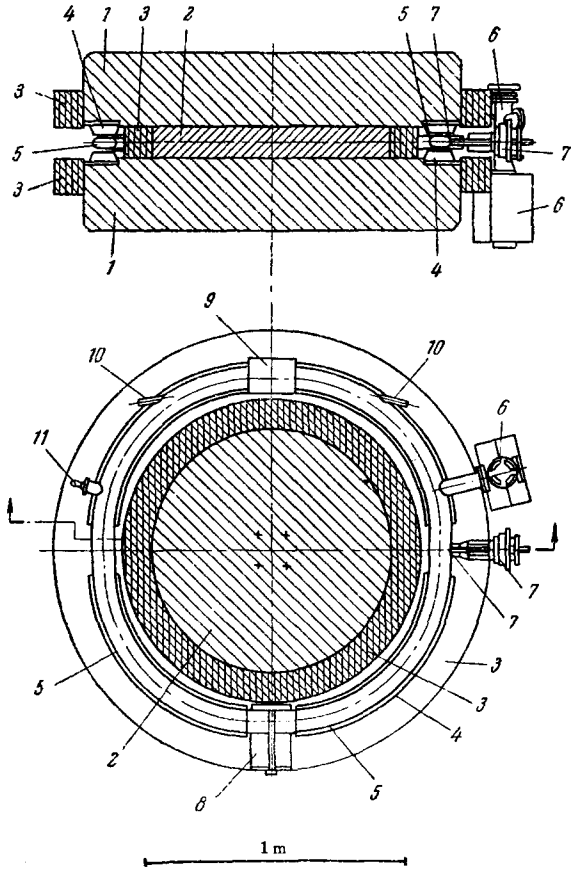

FIG. 11. Diagram of the AdA installation. 1 – Upper and lower armatures of the magnet; 2 – magnet core; 3 – winding; 4 – pole pieces; 5 – vacuum chamber; 6 – titanium pump; 7 – target; 8 – resonator; 9 – gap for experiments; 10 – viewing window; 11 – manometer.

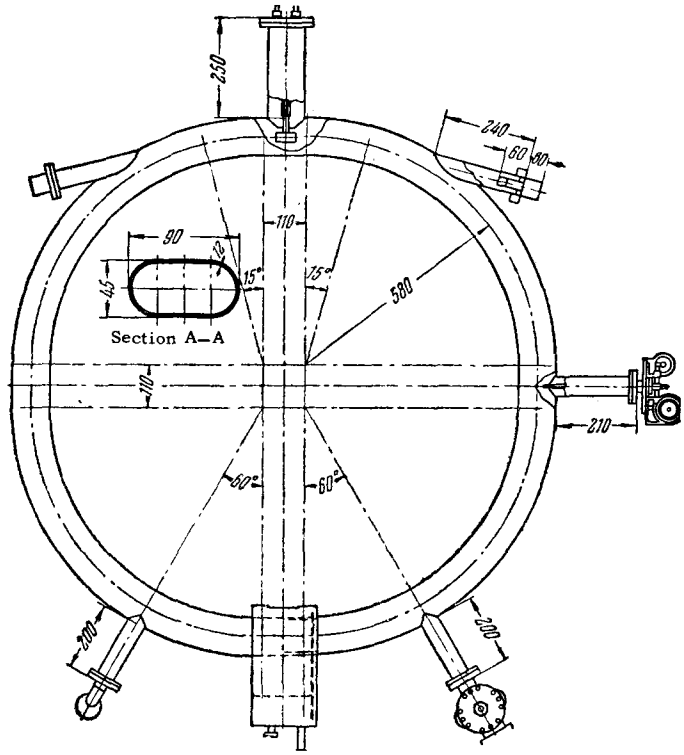

FIG. 12. One of the variants of the AdA storage ring vacuum chamber. In the upper parts of the figure is shown the location of the magnetic inflector, which was subsequently removed.

subdivided in this case into eight sections, in each of which the temperature was stabilized by external means. The diffusion pump was then separated from the chamber, and replaced by a titanium three-electrode Varian pump with rating of 75 liter/sec, which produced after a short pumping time a vacuum of 10^{-9} mm Hg. The best vacuum produced in the AdA chamber was 2×10^{-10} mm Hg.

After the working vacuum was reached, the chamber was installed in the gap of the electromagnet and the evacuation was continued during the entire period of the planned experiments.

The radiation losses in the AdA amounts to 580 eV/rev. They are compensated by a high-frequency field produced by a cavity resonator (Fig. 13) operating at 147 Mc. The resonator is fed from a separately-excited oscillator.

The dimensions of the straight-line gap greatly limit the dimensions of the resonator. For this reason, in order to produce a resonator designed for approximately two meter wavelength with dimensions on the order of $13 \times 20 \times 30$ cm, it becomes necessary to introduce a large lumped capacitance. This greatly reduces the Q of the resonator. For the AdA resonator shown in Fig. 13, the Q was 600, and the shunt resistance was $R_{sh} = 60$ kilohm. The amplitude of the high frequency voltage in the resonator gap reached 10 kV.

Inasmuch as the multiplicity of the high frequency is 2, the chamber contains two clusters of electrons and two clusters of positrons. There are thus on the orbit four points of encounter between the electron and positron clusters, situated in the four straight-line gaps. One of the gaps is occupied by the resonator and the other by the target. The two remaining gaps are assigned for the experiments.

The injection into the AdA is effected in the following manner. The storage ring is mounted on a special rotating support (Fig. 14) and is placed in the path of the photon beam from the synchrotron of electron energy 1 BeV (Fig. 15). The distance between the synchrotron and storage ring targets is 360 cm. A camera for photography of the position of the photon beam on the AdA target and a quantum meter for the measurement of the integrated photon-beam dose produced by the synchrotron are located along the continuation of the photon-beam path. The photon beam creates e^+e^- pairs on a tantalum target $1/10$ radiation unit thick, located in the storage-ring chamber at a distance of approximately 2.5 cm to the outside from the equilibrium orbit. The electrons or positrons (depending on the direction of the field in the storage-ring magnet) contained within a definite interval of input coordinates, angles, and energies, are thus captured in the storage mode.

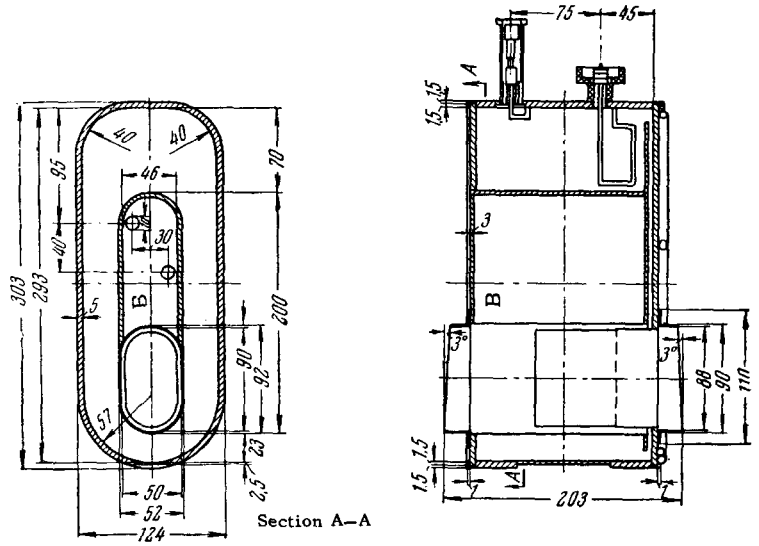

FIG. 13. Resonator of the AdA storage ring. Volume B is a water-cooled radiator which cools the resonator with running water.

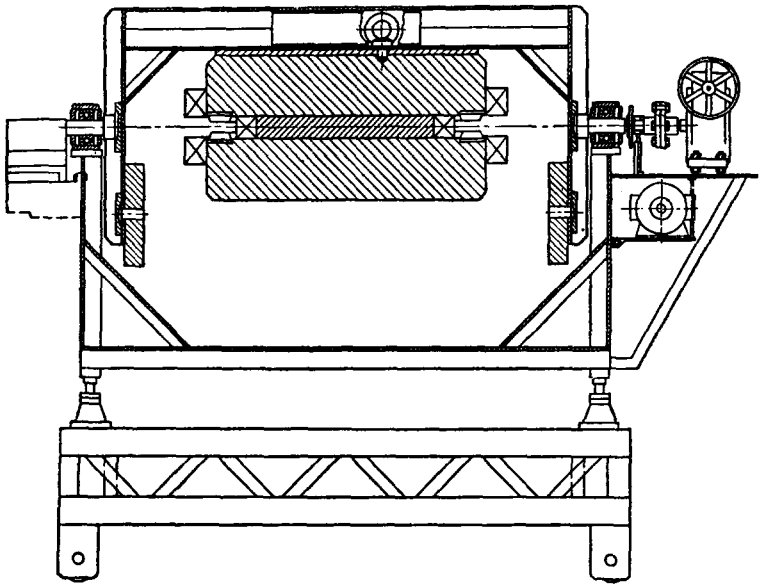

FIG. 14. Mounting of the AdA storage ring on a rotating frame.

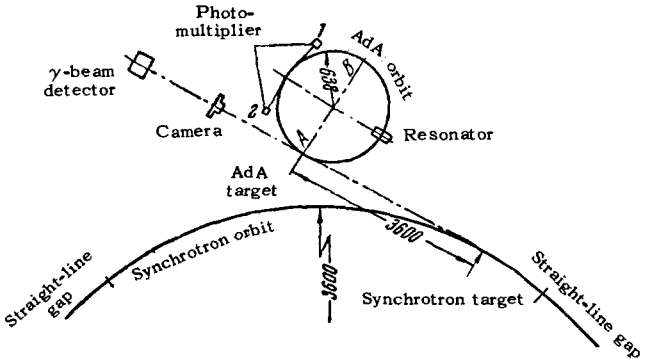

FIG. 15. Arrangement of the AdA storage ring along the path of the photon beam from the Frascati synchrotron.

When the accumulation of particles of one sign terminates, the storage ring together with the beam circulating in its chamber is rotated 180° about the horizontal axis AB, which is perpendicular to the photon-beam direction, and accumulation of particles of the opposite sign begins. Figures 16 and 17 show the storage ring in horizontal and vertical positions.

Bypassing of the target by the injected particles is ensured by a 35% negative modulation of the high-frequency field during 30 microseconds following the entry of the photon beam into the storage-ring target [77]. Particles with energies somewhat above equilibrium move away from the target under the influence of the uncompensated radiative losses, with a velocity which is 50 times larger than that due to the radiative damping of the radial oscillations alone. At the same time, the modulation does not give rise to any noticeable losses of the accumulated beam. An attempt to use a pulsed magnetic inflector to increase the injection efficiency did not increase the capture noticeably.

The capture coefficient turned out to be quite critical to the position of the working edge of the target. A

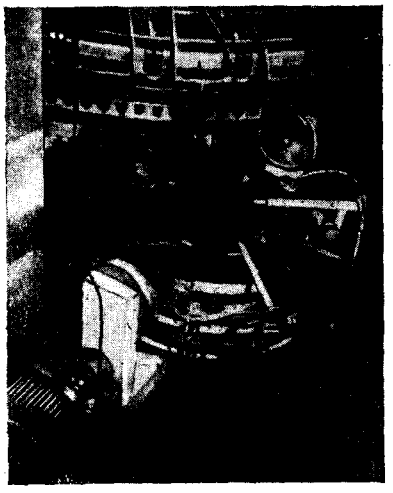

FIG. 16. AdA storage ring in working position.

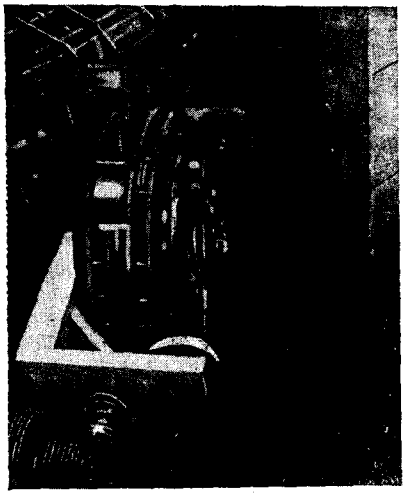

FIG. 17. AdA storage ring at the instant of rotation to change over to accumulation of positrons.

slight tilting of the edge in the radial plane leads to a strong deterioration of the capture.

It is clear from the foregoing that the AdA has in fact no special injection devices. The injection mechanism reduces to a "sampling" on the part of the storage ring of particles with acceptable deviations of the coordinates and momenta, from all the particles formed on the target by the photon beam. The capture coefficient is therefore relatively low. With 10^{11} electrons striking the synchrotron target per second, the best capture coefficient in the storage ring was found to be approximately 300 electrons/sec. Nonetheless, the injection method used in the AdA, in view of its exceeding simplicity, has made it possible to obtain successfully two beams in a single magnetic system with a lifetime of several times 10 hours. Indication of the AdA beam is accomplished by registering the synchrotron radiation with a photomultiplier and using an automatic recorder. The sensitivity of the system made it possible to observe the loss or acquisition of a single electron. This system was used to measure the average lifetime, with the best attainable results being approximately 40 hours.

The rate of accumulation of beams in the AdA when the injection is from the Frascati synchrotron is insufficient for experiments with colliding beams. In view of this fact, the storage ring has been moved at present to Orsay (France) and coupled to the beam of a linear accelerator, where capture of up to 8000 electrons/sec is expected. The main purpose of the physical experiments with the AdA is the investigation of two-quantum annihilation. To this end, two spark chambers were installed in the straight-line gap above and below the vacuum chamber. In a direction tangent to the orbit, Cerenkov counters are placed on both sides of the experimental straight-line gap for the measurement of the secondary-particle energy.

The expected rate of interaction of the beams at 250 MeV and with 1.6×10^7 particles in each beam is $W_1 \approx 0.85$ event/min for the process $e^+ + e^- = 2\gamma$.

The main parameters of the storage ring are listed in the summary table VI.

3. Design of Large Storage Ring of the Frascati National Laboratory (Adone)

The design of the Adone storage ring* provides for two stages. The first is the construction of a storage ring for 750 MeV. Then, on the basis of the information obtained during the realization of this installation, a storage ring for 1.5 BeV is to be constructed[78,79].

A diagram of the Adone storage ring is shown in Fig. 18. The magnet consists of 8 periods. Each period has a structure $\frac{1}{2}OQ_FB2Q_DBQ_F\frac{1}{2}O$, where O — straight line gap, Q_F — quadrupole focusing along the radius, B — turning magnet with weak focusing, Q_D — quadrupole that defocuses along the radius. The choice of such a structure is due to the need for ensuring damping of the radial betatron oscillations and the desire to facilitate the regulation of the betatron frequencies as the beams accumulate. The oscillations are damped because the value of n in the turning magnets is chosen to be equal to 0.5. Indeed, it follows from (3.10) that in this case $\beta_\varphi = 2\lambda_2$, and the damping times of the radial betatron, vertical betatron, and synchrotron oscillations are connected by the equalities $\tau_r = \tau_z = 2\tau_\varphi$[81]. Other variants of the magnetic structure, ensuring damping of oscillations of all three types, were also considered[80,81].

During the course of beam accumulation, the interaction between beams will cause the betatron frequencies to change and approach the resonant values. By varying the current in the quadrupoles it is possible to maintain the betatron frequencies within the specified limits.

The magnetic field on the equilibrium orbit in the turning magnets is assumed equal to 10,000 Oe. At 750 MeV energy it produces a radius of curvature of

*Adone – untranslatable word, denoting the superlative of the word AdA.

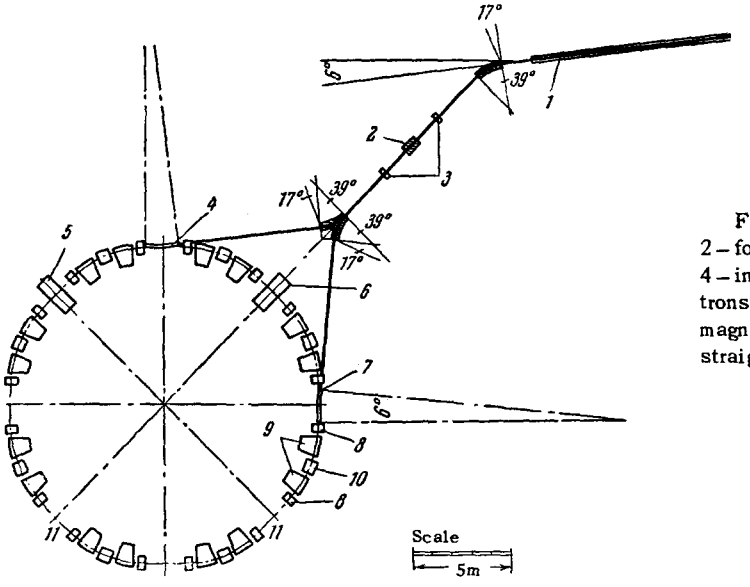

FIG. 18. Diagram of Adone storage ring. 1 – Linear accelerator; 2 – focusing system for electrons; 3 – focusing system for positrons; 4 – inflector for positrons; 5, 6 – resonators; 7 – inflector for electrons; 8 – quadrupole lens focusing along the radius; 9 – turning magnet; 10 – quadrupole lens defocusing along the radius; 11 – straight-line gaps intended for the experiments.

2.5 meters. The lengths of the quadrupoles Q_F and Q_D are 0.5 and 0.4 meter, respectively. The length of the linear gaps is 2 meters. In addition, there are gaps of 15 centimeters each between all elements of the magnetic structure. As a net result, the average radius of the ring is 8.1 meters.

The focusing action of the quadrupoles is given by the parameter $K = G/H\rho_0$, where G is the field gradient in the lenses. The assumed values $K_F = 0.59$ m^{-2} and $K_D = -0.63\,m^{-2}$ ensure $M\nu_r = 2.16$ and $M\nu_z = 2.10$ betatron oscillations per revolution, respectively. The dimensions of the working region of the magnetic field in radius and in height are chosen to be 22 and 9 cm. The permissible energy spread $\Delta E/E$ is $\pm 0.5\%$. The phase area corresponding to capture in the betatron oscillation mode is 10^{-3} rad-cm.

The magnetic field of the turning magnets can be varied within limits corresponding to a change in particle energy between 250 and 750 MeV. This makes it possible to set up experiments over a wide energy range.

The only correcting devices in the Adone are the quadrupole lenses. The quadratic nonlinearity expected with the chosen magnetic system is small, and no correction for it is provided.

The Adone will have two high-frequency resonators operating at 12 Mc. The presence of two resonators makes it possible to prevent loss of the beams in the case of short-duration failures of the high-frequency field in one of the resonators. A model of the Adone resonator (Fig. 19) was constructed and tested in the operating mode. The Q of such a resonator at 19 Mc* turned out to be 3500, and the shunt resistance approximately 90 kilohm. Special discs, which produced an additional capacitance of approximately 400 pF on each side at the end surfaces of the resonator, have made it possible to make the resonator diameter small (2.4 m) with a wavelength of 15.8 m. The output stage of the high-frequency oscillator is located on the resonator directly.

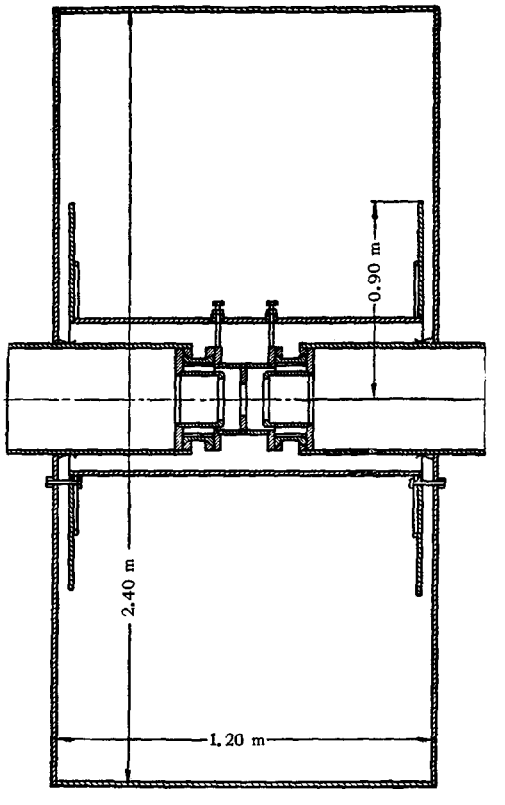

FIG. 19. Model of the Adone resonator.

The particle radiation loss per revolution is 11.5 keV at 750 MeV. The voltage amplitude per revolution is 40 kV.

In the real Adone resonator the vacuum will be pro-

*The model was constructed for 19 Mc because at first the dimensions of the Adone ring were planned somewhat smaller.

duced only in the transit part of the resonator. To this end, as can be seen from Fig. 19, the main volume of the resonator is separated from its central part by quartz tubes.

The volume of the Adone vacuum chamber will apparently be approximately 1500—2000 liters. To ensure an average electron lifetime on the order of 30 hours it is necessary to produce an average of $p = 10^{-9}$ mm Hg along the vacuum orbit. A special problem in this case is the heating of the chamber, which is installed in the electromagnet gap. By means of preliminary electric polishing, heat treatment in a hydrogen medium, and also by using special sorts of stainless steel, it is proposed to reduce the chamber heating temperature to 200°C.

The evacuation of the chamber in the operating mode will be by 16 titanium Varian-type pumps each rated at 400 liters per second. The pressure drop from 10^{-6} mm Hg in the volume of the injection channel to 10^{-9} mm Hg in the Adone chamber is accomplished by constructing part of the injection channel in the form of a tube 20 millimeters in diameter and approximately 1 meter long, with three titanium pumps rated at 100 liters per second each installed along this section.

The most complicated engineering problem is the injection. It is proposed to realize the injection in the Adone at an energy of 400—500 MeV. After the end of the accumulation of the required number of particles, the energy will be increased to the level necessary for the experiment, by slowly increasing the magnetic field. Such an operation, carried out with the AdA, entailed no noticeable loss of particles.

In the Adone storage ring use is made of an inflector variant located outside the equilibrium orbit. The inflector (Fig. 20) consists of four busbars, connected in parallel pairwise. Along the busbars are placed a series of plates, which increase the distributed capacitance of the line and which reduce its wave resistance. One end of the line is connected to the pulse source,

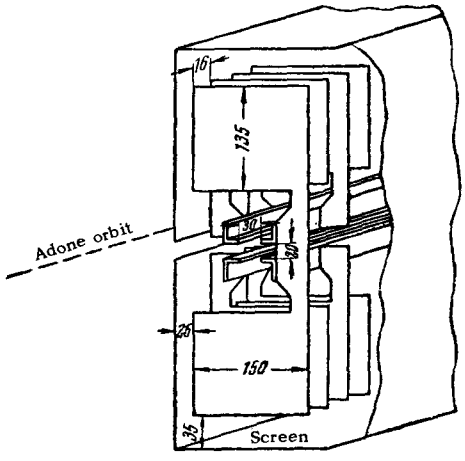

FIG. 20. Model of the Adone inflector.

and the other is loaded by a resistance equal to the wave resistance. A total of 97 L_0C_0 cells are placed along the entire length of the inflector, $l_i = 1.7$ m. The inductance and capacitance of each elementary cell are respectively $L_0 = 8.4 \times 10^{-9}$ H and $C_0 = 40$ pF, with the wave resistance being $R_0 = 15$ ohms. The time of propagation of the wave along the line is 55 nsec. The angle of rotation of the inflector is ~ 0.1 rad. For the injection of particles with energy 500 MeV, the magnetic field should be on the order of 1000 Oe.

To reduce the perturbations in the motion of the accumulated beams by the stray field, the inflector is placed in a screen. The wall of the screen facing the equilibrium orbit has a slot so that the particles that reach the inflector region after several revolutions are not lost on its wall. The time of revolution of the electron in the Adone is 0.16 μsec. The injection will last approximately three revolutions, while the injected particles pass as a result of the oscillations far from the inflector. After the lapse of this time, the magnetic field is turned off. Thus, the inflector will be fed with current pulses of approximate duration 0.5 μsec with fronts on the order of 30—50 nsec. The stability of the field during the duration of the pulse is 1%. The spatial inhomogeneity of the inflector field in a region 1×1 cm^2 likewise does not exceed 1%.

The chosen structure of the electromagnet has the advantage that in the straight-line gap, where the inflector is situated, the envelope of the betatron radial oscillations has a maximum. Because of this, for a specified width of the vacuum chamber, the inflector can be located farther away from the equilibrium orbit and the perturbations of the accumulated beams by the inflector pulse reduced. At the same time, owing to the minimum of the envelope of the vertical oscillations at the azimuth of the inflector, the height of the slot cut in the screen can be decreased and consequently the sagging of the field in the region of the orbit reduced.

Figure 18 shows schematically the equipment of the injection channel. When the inflector 4 is in operation, a set of quadrupole lenses 3 is turned on, while when the inflector 7 operates, set 2 is turned on. In each case the injection optical system is achromatically tuned.

The Adone injector will be a linear accelerator (Fig. 21), the first stage of which will be adjusted for 0.5 BeV energy. The linear accelerator consists of two steps. The first step is designed for acceleration

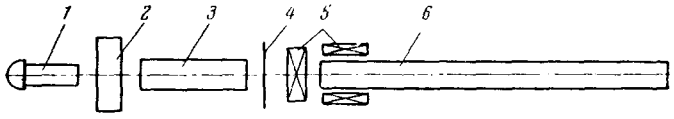

FIG. 21. Diagram of the Adone injector. 1 – Electron gun; 2 – buncher; 3 – first stage of linear accelerator; 4 – converter target; 5 – focusing system; 6 – second stage of linear accelerator.

Table IV

Parameter	Variant I		Variant II	
	Stage 1	Stage 2	Stage 1	Stage 2
Maximum energy, BeV	0.5	2	0.5	2
Average electron current, μA	11	15	26	36
Electrons/sec		$9 \cdot 10^{13}$		$2.2 \cdot 10^{14}$
Pulsed electron current, mA	36	50	57	80
Relative energy spread at half height of the spectrum, per cent		±1.5		±1.5
Current in pulse within the limits ΔE/E = ±0.5% mA		20		32
Maximum pulse duration, μsec	1	1	1.5	1.5
Repetition frequency, cps	300	300	300	300
Reciprocal of duty cycle	$3 \cdot 10^{-4}$	$3 \cdot 10^{-4}$	$4.5 \cdot 10^{-4}$	$4.5 \cdot 10^{-4}$
Number of klystrons	6	33	7	40
Pulse power of klystron, MW	18	18	18	18
Number of accelerating sections	12	33	14	40
Length of section, meters	6	6	5	5
Total length of accelerator, meters	78	215	77	220

of large currents, on the order of 0.5—1 A, to an energy of 30 MeV. Following the strong-current step is located the converter target; which is placed in the beam if it is desired to obtain positrons at the output of the injector. The positrons from the converter target are focused and then accelerated to 0.5 BeV in the second step of the linear accelerator, after which they are directed to the storage ring. The beam injected into the first step of the accelerator from the gun is first bunched with a frequency of 12 Mc. This makes it possible to capture into the accumulation mode practically the entire current of the linear accelerator.

It is proposed to increase the linear accelerator subsequently to an energy of 2 BeV, so as to be able to use it for other experiments and possibly as an injector for a 1500 MeV storage ring. The final parameters of the linear accelerator have not yet been determined. Table IV lists possible variants.

Calculations show[78] that for a storage ring with a specified energy the accumulation time, determined essentially by the rate of accumulation of the positrons, depends on the product $E_i^3 i_+$, where E_i is the injection energy and i_+ is the current of positrons injected in each pulse. Figure 22 shows the pulsed positron current necessary to obtain an accumulation time of 30 minutes, as a function of the injection energy, for two variants of the Adone storage ring.

In the 750-MeV installation, the already considered cluster interaction effects (Sec. 6, Chapter III) make it possible to accumulate only 1 mA of current in each

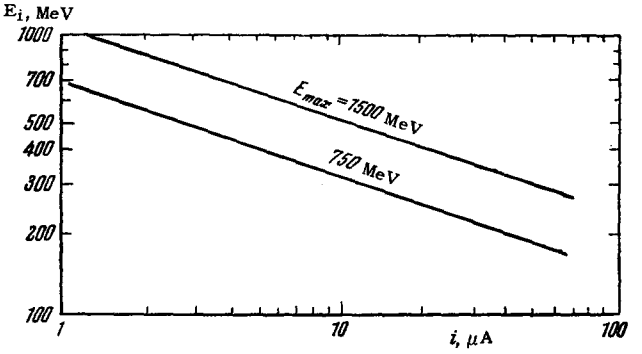

FIG. 22. Injection energy E_i as a function of the positron current of the injector i_+ for different energies of the Adone storage ring and for an accumulation time of 30 minutes.

beam. To increase the accumulated current to ~ 100 mA, the electron and positron beams will be guided along mutually intersecting trajectories, so that their interaction will be weaker. To this end a series of capacitors will be placed along the azimuth of the machine, producing a vertical field of ~ 200 V/cm. By varying the capacitor voltage it will be possible to change the angle and azimuth of intersection of the beams.

Estimates of the dimensions of the clusters yield the following values for the 750-MeV storage ring: $d_\varphi = 60$ cm; $d_r = 0.24$ cm, and $d_z = 1.4 \times 10^{-3}$ cm. If the angle of intersection of the beams is $\delta \approx 2 \times 10^{-3}$ rad, then with $N_+ = N_- = 10^{11}$ particles on the orbit, the "transmission" R is approximately 7×10^{33} $cm^{-2}\ hr^{-1}$. The rates of interaction of the particles in the intersecting beams, for different reactions, are listed in Table V.

The main parameters of the Adone storage ring are listed in Table VI.

4. Geneva Electron Storage Ring

The European organization for nuclear research (CERN) has considered the question of constructing a colliding-proton-beam installation with an energy of approximately 28 BeV.

To investigate a machine of this type, the construction of an electron storage-ring model for 2 MeV is presently nearing completion at CERN[82].

The construction of the model is chosen so as to reflect as much as possible the operating features of a proton storage ring. In particular, at an electron

Table V

Reaction	σ, cm^2	W_1, events/hr
2γ	$8 \cdot 10^{-31}$	5000
$\mu^+ + \mu^-$	$3 \cdot 10^{-32}$	200
$\pi^+ + \pi^-$	$7 \cdot 10^{-33}$	50
$K + \bar{K}$	$3 \cdot 10^{-33}$	20

Table VI. Summary table listing the parameters of storage rings for electrons and positrons

Parameters	Stanford storage ring	Frascati AdA	Frascati Adone	Geneva storage ring
Beams	e^-e^-	e^+e^-	e^+e^-	e^-
Energy, MeV	500	250	750	2
Type of focusing	Weak, but with variable gradient	Weak	Mixed	Mixed
Intensity of magnetic field on the orbit in the turning magnet, Oe	12 000	14 000	10 000	133
Radius of curvature, m	1.4	0.58	2.5	0.6
Average radius, m	1.85	0.64	8.1	3.8
Number of periods of the magnetic structure	4 (per ring)	4	8	12
Number of turning magnets	4 (per ring)	4	16	12
Length of arc of turning magnet, m	1.57 1.05	0.9	0.98	0.4
Fall-off exponent of magnetic field in turning magnet	0	0.6	0.5	0
Number of straight-line gaps	7 (for two rings)	4	8	12
Length of straight-line gap, m	0.7	0.18	2	0.8
Number of quadrupole lenses	–	–	16 focusing 8 defocusing	12 focusing 12 defocusing
Length of quadrupole lenses, m	–	–	focusing, 0.5 defocusing, 0.8	0.3
Gradient in quadrupole lens, Oe/cm	–	–	focusing, +148 defocusing, −158	7.6
Dimensions of working region of magnetic field, cm^2	13×5	6×3	22×9	9.5×4.2
Weight of iron of electromagnet, tons	43	7.7		6
Weight of copper of main winding, tons	3	0.5		0.5
Power consumed by electromagnet, kW	450	100		0.1
Number of radial betatron oscillations per revolution	0.8	0.63	2.16	2.75
Logarithmic derivative of the length of the orbit with respect to the momentum	–	–	0.192	0.138
Permissible energy spread of storage ring, per cent	±0.6	±0.25	±0.5	±0.25
Damping time, sec	$3\cdot10^{-3}$	$7\cdot10^{-3}$	$22.8\cdot10^{-3}$	
Azimuthal length of cluster, cm	60		60	
Width of cluster, cm	0.5		0.24	
Height of cluster, cm	$\sim5\cdot10^{-3}$	$\sim2.5\cdot10^{-3}$	$\sim1.4\cdot10^{-3}$	
Number of particles in each beam	$\sim3\cdot10^{11}$	$3\cdot10^{7}$	$1\cdot10^{11}$	
Circulating current of each beam, mA	~1500	0.36	100	
Time of one revolution, sec	$2.76\cdot10^{-8}$	$1.34\cdot10^{-8}$	$0.16\cdot10^{-6}$	$8.3\cdot10^{-8}$
Number of resonators	2 (per ring)	1	2	1
Frequency, Mc	36.3	147	12.5	24.2
Multiplicity	1	2	2	2
Amplitude voltage in resonator, kV	40	10	20	0.01
Energy loss per revolution, keV	5	0.58	11.5	–
Equilibrium phase, deg	86.4	86.6	73	~90
Q of resonator	5000	600	~3500	
Power consumed by high-frequency system, kW	60			
Injector	Linear accelerator	Synchrotron or linear accelerator	Linear accelerator	Van-de-Graaff generator
Injector energy, MeV	500	150–250	400	1.75
Electron current of injector in pulse, mA	25		30–50	1500
Type of inflector	Pulsed ferrite magnet	–	Pulsed magnet without core	Pulsed ferrite magnet
Pulse voltage on inflector, kV	25	–	90	17
Pulse current of inflector, A	7500 (for three sections)	–	6000	
Characteristic resistance of inflector, ohm	10	–	15	
Inflector pulse power, MW	190	–	550	
Length of plateau of inflector pulse, sec	$6\cdot10^{-8}$	–	$5\cdot10^{-7}$	$8\cdot10^{-8}$
Duration of inflector pulse fronts, sec	$\sim5\cdot10^{-8}$	–	~3–$5\cdot10^{-8}$	$\sim8\cdot10^{-9}$
Injection pulse repetition frequency, cps	60	50		50
Time of accumulation of nominal current, sec	80	From synchrotron, 10^5, and from linear accelerator, 5×10^3	$3\cdot10^3$	
Number of titanium pumps		1	16	12
Per activity of titanium pump, liters/sec		75	400	140
Design vacuum, mm Hg	10^{-9}	$5\cdot10^{-10}$	10^{-9}	10^{-9}
Average lifetime of beam, hr	30	40	30	$3\cdot10^{-3}$

energy of 2 MeV, the magnetic field on the equilibrium orbit is taken equal to 133 Oe. Therefore the electron radiation losses are negligible and cause no change in the oscillations of the electron relative to the equilibrium orbit. The storage-ring magnet constitutes a system of 12 periods, each of which (Fig. 23) includes a turning magnet and two quadrupole lenses with gradients of opposite signs[83]. The total length of the ring along the central orbit is 24 meters.

The storage-ring injector is a Van-de-Graaff generator with two accelerating tubes. The beam of one of the tubes is injected into the ring, while the second beam is used to regulate the injector energy in accordance with the field of the turning magnets. To this end a sector magnet, analogous to the turning magnet of the periodic structure of the ring, is placed along the path of the second beam. Its winding is connected in series with that of the ring magnet. When the field in the ring magnet changes, the beam at the output of the sector magnet is deflected and signals for a change in the repetition frequency of the beam from the second accelerator tube. This changes the voltage on the common conductor of the Van-de-Graaff generator and consequently the energy of the injected beam.

The injected beam is brought into the ring from the inside with the aid of a pulsed ferrite inflector. Inasmuch as the oscillations are not damped in this machine, to repeat the inject cycles it is necessary to deflect the beam away from the inflector to a distance where it is not subject to the influence of the inflector field. To this end, once the captured electrons are bunched into a cluster, the accelerating frequency is reduced by approximately 0.5%, and the captured cluster is shifted to an external radius[85]. Because of this, the next injection act does not disturb the previously accumulated beam.

Inasmuch as there are practically no radiation losses, a voltage with 10 V amplitude on the resonator gap produces a sufficiently wide region of phase-oscillation stability.

The vacuum chamber (Fig. 24) is pumped out with the aid of 12 titanium pumps rated at 140 liters per second. It is outgassed by heating it to t = 300°C. In order to prevent heating of the magnet, the chamber is cooled with running water flowing under a special jacket, so that the temperature of the poles does not rise by more than 1°C.

The flange gaskets are provided with gold liners. Altogether the chamber has 150 gaskets, 400 welded seams, and 40 metal-ceramic seals. The design pressure is 10^{-9} mm Hg.

Inasmuch as the magnetic field of the storage ring

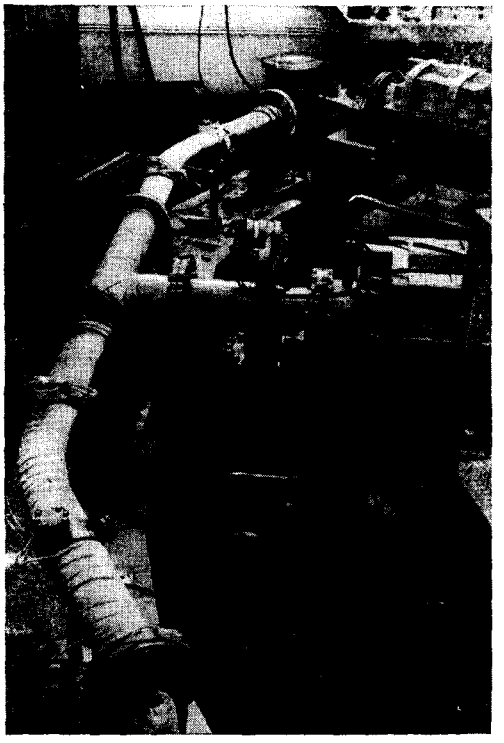

FIG. 24. Part of the vacuum chamber of the Geneva electron storage ring, prepared for heating to produce high vacuum.

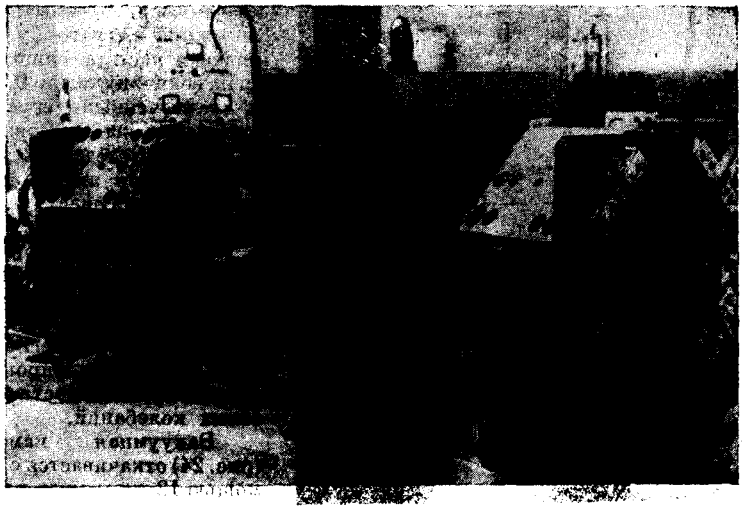

FIG. 23. Period of the magnetic structure of the Geneva electron storage ring.

is small, and the tolerances for its deviation are quite rigorous, all portions of the chamber placed outside the gap of the electromagnet are provided with a magnetic screen. In addition, the room in which the installation is located is screened.

By now (end of 1962) the erection of the electromagnet is complete and the operating vacuum has been produced in half of the ring chamber.

The main parameters of the installation are listed in Table VI[86].

The construction of storage rings for charged particles is widely developing at the present time in many laboratories of the world. In addition to the installations already mentioned, an electron-positron storage ring for 450 MeV is under construction in Saclay (France), and the possibility of constructing storage rings in some other laboratories is also considered. The wealth of information that can be gained from experiments with colliding beams is in full correspondence with the difficulties that must be overcome in order to obtain this information.

[1] R. P. Feynman and G. Speisman, Phys. Rev. **94**, 500 (1954).

[2] R. P. Feynman, Proceedings of the Aix-en-Provence International Conference on Elementary Particles, Saclay, France, 14—20.IX. 1961, v. 2, p. 205.

[3] G. K. O'Neill, Brookhaven Conference, September 1961, p. 64.

[4] G. K. O'Neill, Phys. Rev. **102**, 1418 (1956).

[5] V. A. Petukhov, JETP **32**, 379 (1957), Soviet Phys. JETP **5**, 317 (1957).

[6] W. M. Brobeck, Symposium on High Energy Accelerators, CERN, Geneva, 1956, p. 60.

[7] Lichtenberg, Newton, and Ross, Intersecting Beam Accelerator with Storage Ring, Reports Midwestern Universities Research Association, Madison, Wisc., No. 110, 4.IV.1956.

[8] D. W. Kerst et al, Phys. Rev. **102**, 590 (1956).

[9] D. W. Kerst, Symposium on High Energy Accelerators, CERN, Geneva, 1956, p. 36.

[10] L. W. Jones, Proceedings of the International Conference on High Energy Accelerators, CERN, Geneva, 1959, p. 15.

[11] G. K. O'Neill, Proceedings of the International Conference on High Energy Accelerators, CERN, Geneva, 1959, p. 23.

[12] Yu. F. Frolov, in "Voprosy fiziki elementarnykh chastits" (Problems in Elementary Particle Physics) edited by A. I. Alikhanyan, Erevan, AN ArmSSR, 1962, p. 318.

[13] A. A. Kolomenski and A. N. Lebedev, Proceedings of the International Conference on High Energy Accelerators, CERN, Geneva, 1959, p. 115.

[14] MURA Staff, Proceedings of the International Conference on High Energy Accelerators, CERN, Geneva, 1959, p. 71.

[15] V. N. Baier, see reference 12, p. 337.

[16] L. M. Afrikyan and G. M. Garibyan, JETP **33**, 425 (1957), Soviet Phys. JETP **6**, 331 (1958).

[17] F. E. Low, Phys. Rev. **120**, 582 (1960).

[18] N. Cabbibo and R. Gatto, Phys. Rev. Letts. **4**, 313 (1960).

[19] N. Cabbibo and R. Gatto, On Electron-positron Colliding Beam Experiments, Laboratori Nazionali di Frascati, Nota interna, No. 82, 26.VI.1961.

[20] R. Gatto, On Experimental Possibilities with Colliding Beams of Electrons and Positrons, Laboratori Nazionali di Frascati Nota interna, No. 91, 1.IX.1961.

[21] N. Cabbibo and R. Gatto, Phys. Rev. **124** (5), 1577 (1961).

[22] N. Cabbibo and R. Gatto, Nuovo cimento, Ser. X, **20**, 184 (1961).

[23] V. N. Baĭer, see [12], p. 355.

[24] R. Gatto, Proceedings of the Aix-en-Provence International Conference on Elementary Particles, Saclay, France, 14—20.IX.1961, v. 1, p. 487.

[25] R. Gatto, Proceedings of the International Conference on Theoretical Aspects of Very High-Energy Phenomena, CERN, Geneva, Switzerland, 5—9 June, 1961, p. 75.

[26] S. Drell, Ann. Phys. **4**, 75 (1958).

[27] V. N. Baĭer, UFN **78**, 619 (1962), Soviet Phys. Uspekhi **5**, 976 (1963).

[28] A. A. Kolomenskiĭ, JETP **33**, 298 (1957), Soviet Phys. JETP **6**, 231 (1958).

[29] V. N. Kanunnikov, et al, Proceedings of the International Conference on High-Energy Accelerators, CERN, Geneva, 1959, p. 89.

[30] T. Ohkawa, Rev. Sci. Instr. **29**, 108 (1958).

[31] Yu. M. Ado, Atomnaya énergiya (Atomic Energy) **12**, 54 (1962).

[32] F. Amman, Preliminary Consideration of a Proposal for Colliding Beam Accelerator in the GeV Region (Adone), Laboratori Nazionali di Frascati, Nota interna, No. 79, 6.VI.1961.

[33] D. Bohm and L. Foldy, Phys. Rev. **70**, 249 (1946).

[34] M. S. Rabinovitsch, J. Phys. USSR **10**, 523 (1946).

[35] M. Sands, Phys. Rev. **97**, 470 (1955).

[36] A. A. Kolomenski and A. N. Lebedev, Symposium on High-Energy Accelerators, CERN, Geneva, 1956, p. 447.

[37] A. A. Kolomenskiĭ and A. N. Lebedev, DAN SSSR **106**, 87 (1956).

[38] A. A. Kolomenskiĭ and A. N. Lebedev, JETP **30**, 207 (1956), Soviet Phys. JETP **3**, 132 (1956).

[39] A. A. Kolomenskiĭ and A. N. Lebedev, JETP **30**, 1161 (1956), Soviet Phys. JETP **3**, 946 (1956).

[40] K. A. Symon and A. M. Sessler, Symposium on High-Energy Accelerators, CERN, Geneva, 1956.

[41] V. S. Synakh, JETP **40**, 194 (1961), Soviet Phys. JETP **13**, 134 (1961).

[42] L. Katz and L. H. Lokan, Nuclear Instr. **11**, 7 (1961).

[43] L. Katz, Nuclear Instr. **11**, 14 (1961).

[44] D. Yount and J. Pine, Report High-Energy Physics Laboratory, Stanford University, Stanford, California 249.

[45] S. A. Kheĭfets, see [12], p. 303.

[46] Yu. F. Orlov, PTÉ No. 2, 17 (1959).

[47] G. K. O'Neill, Proceedings of the International Conference on High Energy Accelerators, CERN, Geneva, 1959, p. 125.

[48] Yu. F. Orlov and E. K. Tarasov, JETP **34**, 651 (1958), Soviet Phys. JETP **7**, 449 (1958).

[49] K. W. Robinson, Phys. Rev. **111**, 373 (1958).

[50] Orlov, Tarasov, and Kheĭfets, PTÉ No. 1, 17 (1959).

[51] Orlov, Tarasov, and Kheĭfets, Proceedings of the International Conference on High-Energy Accelerators, CERN, Geneva, 1959, p. 306.

[52] A. A. Kolomenskiĭ, Proc. Phys. Inst. Acad. Sci., vol. 13, no. 3, AN SSSR, 1960.

[53] A. A. Kolomenskiĭ and A. N. Lebedev, Atomnaya énergiya **5**, 554 (1958).

[54] S. A. Kheĭfets, PTÉ No. 6, 18 (1960).

[55] Yu. F. Orlov and E. K. Tarasov, PTÉ No. 5, 17 (1958).

[56] A. A. Kolomenski and A. N. Lebedev, Suppl. Nuovo. cimento **7**, 43 (1958).

[57] S. A. Kheĭfets, PTÉ No. 6, 18 (1960).

[58] C. Bernardini and B. Touschek, On the Quantum Losses in an Electron Synchrotron, Laboratori Nazionali di Frascati, Nota interna, No. 34, 27.IV.1960.

[59] C. Bernardini, The Z-Distribution of an Electron Beam in a Storage Ring, Laboratori Nazionali di Frascati, Nota interna, No. 145, 20.VI.1960.

[60] M. Barbier, Proceedings of the International Conference on High Energy Accelerators, CERN, Geneva, 1959, p. 100.

[61] A. A. Sokolov and I. N. Ternov, DAN SSSR **97**, 823 (1954).

[62] L. Osborne and D. Ritson, Cambridge Accelerator Project, Report No. 7 (1955).

[63] A. A. Sokolov and I. M. Ternov, JETP **28**, 431 (1955), Soviet Phys. JETP **1**, 227 (1955).

[64] I. G. Henry, Phys. Rev. **106**, 1057 (1957).

[65] C. Pellegrini, Suppl. Nuovo cimento **22**, 603 (1961).

[66] C. Pelligrini, A Calculation of Radiation Effects on Electron Oscillations in a Circular Accelerator, Laboratori Nazionali di Frascati, Nota interna, No. 90, 1.IX. 1961.

[67] F. Amman and D. Ritson, Space Charge Effects in e^-e^- and e^+e^- Colliding or Crossing Beam Rings, Laboratori Nazionali di Frascati, Nota interna, No. 86, 24.VII.1961.

[68] Jahnke and Emde, Tables of Functions (Russ. Transl., M., Gostekhizdat, 1949, p. 97).

[69] E. M. Moroz, ZhTF **33**, 455 (1963), Soviet Phys. Tech. Phys. **8**, 337 (1963).

[70] M. Bassetti, Calcoli numerici sugli effeti di carica spaciale in un anello d'accumulazione per elettroni e positroni, Laboratori Nazionali di Frascati, Nota interna, No. 135, 5.III.1962.

[71] G. K. O'Neill, Bull. Amer. Phys. Soc. **3**, Dz. (1958).

[72] E. J. Woods and G. K. O'Neill, Bull. Amer. Phys. Soc., Ser. II, **3**, 169 (1958).

[73] Barber, Richter, Panofsky, O'Neill, and Gittelman, An Experiment on the Limits of Quantum Electrodynamics, Report of High-Energy Physics Laboratory, Stanford University, Stanford, California, No. 170, June 1959.

[74] O'Neill, Barber, Richter, and Panofsky, A Proposed Experiment on the Limits of Quantum Electrodynamics, Report High-Energy Physics Laboratory, Stanford University, Stanford, California, May 1958.

[75] B. Richter, Proceedings of the International Conference on Theoretical Aspects of Very High-Energy Phenomena, CERN, Geneva, Switzerland, June 5—9, 1961, p. 57.

[76] Bernardini, Corazza, Ghigo, and Touschek, Nuovo cimento, Ser. X, **18**, 1293 (1960).

[77] Bernardini, Bizzarri, Corazza, Ghigo, and Querzoli, Nuovo cimento, Ser. X, **23**, 202 (1962).

[78] Amman, Bassetti, Bernardini, Catoni, Corazza, Evangelisti, Garolla, Pellegrini, and Ritson, Proposta per la realizzazione di un annello di accumulazione per elettroni e positroni da 1.5 GeV, Laboratori Nazionali di Frascati, Nota interna, No. 105, 7.XII.1961.

[79] F. Amman and D. Ritson, Design of Electron-positron Colliding Beam Rings, Proceedings of the Brookhaven Conference, September 1961.

[80] Bassetti, Evangelisti, and Pellegrini, Determinazione dei diversi parametri di una struttura magnetica "Smorzata," Laboratori Nazionali di Frascati, Nota interna, No. 121, 8.III.1962.

[81] L. Mango, Studio dei parametri di una struttura a funzioni separate con focheggiamento forte, Laboratori Nazionali di Frascati, Nota interna, No. 134, 3.III.1962.

[82] Hereward, Johnsen, Schoch, and Zilverschoon, Proceedings of the Brookhaven Conference, September 1961.

[83] M. I. Pentz, Beam Optics of the Storage Ring, Report CERN AR (Int. SR) 62—6, 24.V.1962.

[84] E. Fischer, The Vertical Displacement of the Closed Orbit due to the Clearing Field, Report CERN AR (Int. SR) 61—30, 29.XI.1961.

[85] D. A. Swenson, A Study of the Beam Stacking Process, Report CERN AR (Int. SR) 61—19, 27.VIII.1961.

[86] K. Johnsen, List of Parameters for the S.R. model, Report CERN AR (Int. SR) 61-16, 27.VI.1961.

[87] C. Bernardini et al, Phys. Rev. Letts. **10**, (9), 407 (1963).

Translated by A. M. Bincer and J. G. Adashko